TAILORING FORCE INTERACTIONS FOR SOLVENT-BASED PROCESSING OF CERAMICS

By

KARRAN V. WOAN

A DISSERTATION PRESENTED TO THE GRADUATE SCHOOL
OF THE UNIVERSITY OF FLORIDA IN PARTIAL FULFILLMENT
OF THE REQUIREMENTS FOR THE DEGREE OF
DOCTOR OF PHILOSOPHY

UNIVERSITY OF FLORIDA

2011

To the University of Florida Department of Materials Science and Engineering

ACKNOWLEDGMENTS

I thank my family for providing me with the opportunity and life to be able to focus on making a difference. I would also like to thank my closest friends (Andy Gerger, Ron Jones, Hyoungjun Park, Derek Rampal, and Morgan Yorloff Richardson) for fostering kindness and patience. Especially, I was assisted and trained in various research techniques by Georgios Pyrgiotakis. Finally, I thank all my colleagues, my mentor, the UF Department of Materials Science and Engineering, and all those educators who I've been blessed to have had for guidance in becoming a more professional and effective scientist and engineer.

TABLE OF CONTENTS

page

LIST OF TABLES

LIST OF FIGURES

LIST OF ABBREVIATIONS

AES	Auger electron spectroscopy
AFM	Atomic force microscopy
DLVO	Derjaguin and Landau, Verwey and Overbeek theory
DRF	Dielectric response function
EDL	Electric double layer
HPLC	High performance liquid chromatography
OTS	Octadecyltrichlorosilane
PTFE	Polytetrafluoroethylene
SEM	Scanning electron microscopy
SFA	Surface force apparatus
THF	Tetrahydrofuran
vdW	van der Waals
VOC	Volatile organic compounds
XRD	X-ray diffraction

Abstract of Dissertation Presented to the Graduate School
of the University of Florida in Partial Fulfillment of the
Requirements for the Degree of Doctor of Philosophy

TAILORING FORCE INTERACTIONS FOR SOLVENT-BASED PROCESSING OF CERAMICS

By

Karran V. Woan

May 2011

Chair: Wolfgang M. Sigmund
Major: Materials Science and Engineering

Environmental pollution resulting from burn-off is a major concern during ceramics processing. Focus on decreasing organic content and increasing recovery of solvents has become very desirable both from a manufacturing plant standpoint as well as from the standpoint of the government and its people. Colloid processing advances using atomic force microscopy is presented as a means to develop a solvent-based system through which interactions of particles in suspensions with the wall or with themselves can be tailored without the use of organic dispersants. Predictions are made and expected force interactions are calculated for silica particle interactions with a steel wall under various liquid environments. Attachment of a colloid sphere atop of an AFM cantilever allows for the measurement of interaction between the sphere and a surface. Van der Waals interactions in aqueous and non-aqueous environments are specifically calculated and addressed and the effect of porosity is compared with the idealized solid-sphere case. Furthermore, development of methodologies to examine force interactions of particles (both hydrophobic and hydrophilic) in solvents is detailed.

CHAPTER 1
INTRODUCTION

Ceramics Processing

Ceramics form some of the hardest and most stable materials known to man. The chemical combination of a metal with a nonmetal through covalent and ionic bonds impart these properties. The lack of chemical reactivity and extreme hardness are often times what make these materials desirable, resulting in the use of the materials in such applications as refractory, culinary, storage, structural, and shielding. However, these same properties make the materials quite challenging to process.

Traditionally, and in the realm of art, finished ceramic works were completed in a variety of ways. There's the traditional act of chiseling and carving which can be applied to sculptors who utilize everything from chisels to chainsaws when shaping and forming intricate designs and structures from large blocks of raw materials. These materials can extend from marble, to granite, to jade, and even to ice.

Another way in which ceramics have been shaped is through the process of building upwards or consolidation. This applies to such arts as pottery or glass-forming. In glass forming, hard pieces of silica are heated upwards of 1300°C and then blown into intricate shapes and allowed to gradually cool to remove residual stresses. In pottery, clay particulates are watered down and made into a pliable paste and then molded to shape. Ceramic figurines can also be made from clay casted into shapes by designed molds or templates. The final product is either fired in a kiln or glazed over with a silica-type compound before firing. The firing causes the individual particles to undergo mass transport processes fusing the particles with one another and forming a dense structure.

Though the arts emphasize uniqueness, aesthetics, and often times the addition of proprietary ingredients which yields effects of unknown mechanisms, the scientific and engineering aspects maintains reproducibility and identifying mechanisms and trends as its priority. Significant industries exist for the production of traditional ceramics such as those for white wares, pottery, paper coatings, and refractory applications. Many industrial and technical processes remain an art due in large part to the difficulties of reproducibility and limitations of scientific research capabilities. Often times the art persists in combination of the aforementioned difficulties as well as for the preservation of trade secrets in both materials components and processing.

Furthermore, advanced application ceramics processing techniques began taking shape in the last 50 years. These further applications of ceramic materials include electronics, biomedical, dental and cosmetics, surface coatings, catalytic degradation, and energy production and storage materials. Well defined tolerances and control of purity and reproducibility during processing becomes much more necessary.

Figure 1-1 is of the so called “Materials Science Tetrahedron” which graphically represents the interrelationships between various factors in producing a material for a desired application. In most applications the performance of the material is the bottom-line task for the engineer. This performance includes such factors as how well a material performs its intended task in a particular environment or how frequent a load a material can take. Materials scientists and engineers seek to understand and to utilize the interplay of how synthesis, microstructures, and materials properties affect one another and to design for a certain application or to performance criteria.

Rather than machining out parts like how a sculptor might go about carving ice or chiseling marble into unique works, advanced ceramics are usually processed with similar methodologies to pottery or casting since they allow for significant control for each step of the process. Generally, the processing can be segmented into a variety of steps. The first stage is the acquisition and purification of fine and powdery raw materials. This may be obtained from nature through mining or synthesized in the laboratory. Often times this stage requires very well characterized particles of particular sizes and shapes and levels of purity for the intended application.

The second stage consists of forming and or consolidation of the particles. This may be achieved through pressing, casting into a mold, plastic forming, injection molding, and various other processes, which yields a desired shape. These varieties of processing techniques often require the use of some sort of mechanism to fluidize the particles and allow them to take upon a desired geometry. In some applications this filling or shaping stage is the final and intended product such as in chromatographic columns or in filtration vessels containing particulate matter.

The final step often consists of heating or firing the system to facilitate a variety of processes. The first is termed calcination which relates to the chemical decomposition of various carbonate or hydrated minerals, to remove unwanted compounds, or to cause changes in material phases. The second function, and often occurring at higher temperatures, is the sintering process resulting in appreciable mass transport resulting in the fusing of particles and densification of the final product.

Any of these steps can lead to flaws in the final product. Issues with the raw material include non-uniform sizes of particles or contamination and unwanted phases

which can make for difficulties in shaping and further result in non-uniform firing and lead to mechanical failure of the product. Consolidation or shaping issues include large part lines or inability to maintain the shape under its own weight or the presence of stress concentrators like pores which can lead to mechanical failure during the firing stage. Furthermore, inadequate time or temperature effects during firing could lead to an immature final product with stress concentrators due to unreacted components, pore and void formation, formation of unwanted microstructures and large sized defects, or non-uniformity of the finished product.

The shaping or packing stage during which particles are fluidized generates a great deal of challenges and materials science-based research opportunities. Significantly, often times, large amounts of organic dispersants and other additives are utilized to ensure the particles remain in suspension and to ensure uniform fluid properties. For instance, during injection molding processing, the fluidized ceramics may contain nearly 20 volume percent organics.[1] The calcination of these parts leads to combustion of the organics and results in the dispersal of volatile organic compounds (VOC) into the atmosphere.

Environmental Impact of Ceramics Processing

The ceramics industry is responsible for a great deal of particulate air pollution as well as VOCs and sulfur dioxide gas during manufacturing. China produces 2/3rd of the world's total ceramics output.[2] Previously, a major portion of the ceramics industry was located in Guangdong, China's largest (population-wise) and most prosperous province. Unfortunately, the large concentration of ceramics processing (as well as other manufacturing) plants in the city of Foshan led to significant air and water quality issues for the region.

Environmental concern has become more significant with the impact of rapid urbanization and industrialization being felt. The ecosystem and environment just can't keep up with the pace of development, and this has led to some serious repercussions to both China's land and her people. A third of the land experiences acid rain, half of the river waters are not potable resulting in a quarter of the people not having clean drinking water, and finally, air pollution has led to lung cancer being the number one killer of the country's people. These statistics were taken from a "National Strategies and China Ceramics Industry in the Future" trade news article published in the fall of 2010. Though the majority of the acid rain, air particulates, and other toxic pollutants is the result of the energy sector's coal-burning plants, pollution from ceramics production contributes quite significantly to the deterioration of the environment and people's health.[3]

The environmental pollution can be categorized into either air-based or water-based pollutants. Ceramics processing and manufacturing facilities contribute to air pollution through the production of various substances including sulfur dioxide, nitrogen dioxide, ozone, and suspended particulates, the listed being those which are monitored. Reports in 2007 detailing the air quality of the Guangdong province indicate that over a third of the time, the concentrations of pollutants exceeded the government-established thresholds.[4]

Water pollution stems from the water/aqueous-based contribution often used to suspend ceramics raw materials during transport or forming steps of the processing. This waste water often results from the presence of additives to impart good dispersive

qualities. The resulting aqueous solution is no longer useful and is often released into nearby bodies of water before decontamination.

Pollution problems have since been mitigated through logistical handling by shutting down 87 ceramics enterprises and 269 production lines within the Chancheng district in Foshan. Furthermore implementation of technological pollution-mitigating procedures included subjecting exhaust gas to a kiln to further decompose organic compounds, drying the exhaust, desulphurization, and removal of dust have led to decreased environmental impact.[3]

However, most of these steps are instated after waste has already been generated. The manufacturing centers have increasingly sought purer and higher grade raw materials which does cut down on some of the side reactions which might evolve toxic compounds, but to a large extent, the ceramics processing remains the same. And prevention of waste dispersed into the environment is the standard task rather than the minimization of waste generation in the first place.

The focus and goal of this dissertation is to develop characterization techniques that will facilitate an approach to processing which minimizes the use of large amounts of dispersants or other organic lubricants. Furthermore, a system which can be recovered readily and be reused for subsequent batch processing is desired so as to minimize further streams of waste generation.

Objectives and Approach

The goal is to move towards systems which don't depend on excess and unrecoverable additives during processing. Objective-wise, this means developing a liquids-based system and characterization capabilities and protocol to reinforce and support its design. The approach is to utilize the advances that have been made in

colloidal science processing to predict and tailor interactions between ceramic particles and various interfaces during processing. Predictions occur through the use of simplified theories of force interactions at a distance between surfaces in various media, and direct characterization occurs by modified atomic force microscopy to quantify the interaction forces experienced between two real world surfaces in a variety of liquid media and to compare the results with theory.

Structure of Thesis

Now that an impetus for developing processes to minimize the use of large organic processing aids has been established, Chapter 2 provides the background information and literature review on the topic of force interactions between surfaces in colloidal systems and larger suspensions, primarily as it relates to ceramics processing. A discussion on the mechanisms of fundamental forces between surfaces is presented and methods to calculate and to predict the interactions are addressed. Detailed developments of characterization techniques to quantify surface forces in liquid environments are provided. Chapter 3 addresses the surface properties of a model materials system. Further calculation and use of theory to predict expected interactions are provided. This is followed by detailed modifications to the AFM liquid cell to expand its versatility towards a greater variety of liquid media and the construction of the colloid probes in Chapter 4. Chapter 5 provides experimental parameters to both characterize the colloid probe interaction area and the cantilever spring constant as well as the experimental parameters and results of the colloid probe measurement technique in liquid media of interest. Analysis and discussion of the results in the context of literature is also provided. Furthermore, consideration is placed on the effect of solvent selection on particle-particle interactions. Chapter 6 provides some conclusions and elaborates

on extensions and future work to facilitate the characterization of particle-particle interactions using colloid probe AFM and to further develop science-based solvent selection and characterization methods.

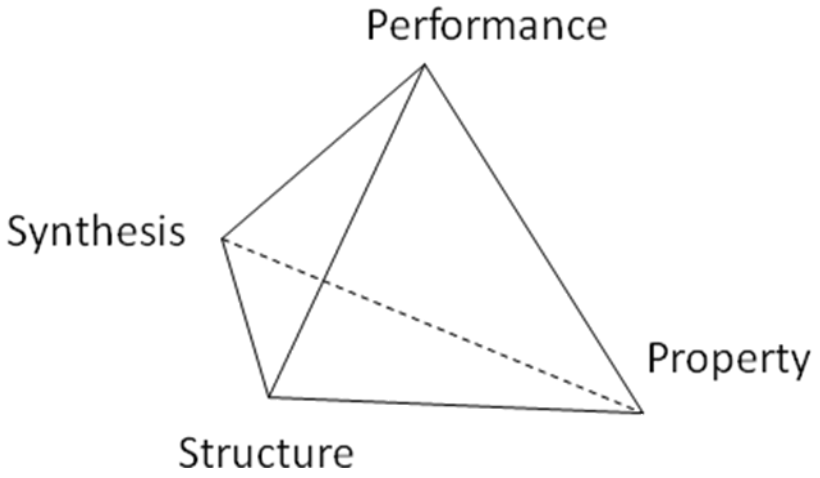

Figure 1-1. Materials science tetrahedron demonstrating the interplay between synthesis, structure, property, and the resulting performance.

CHAPTER 2
BACKGROUND

Colloidal Science and Particle Dispersions

Colloids are mixtures of two or more phases. One phase forms the continuous or host matrix while the second phase is the dispersed or particulate medium. The immiscible combinations of solids, liquids, and gases in one another are often provided unique terms. A liquid phase dispersed or as a continuous phase in a solid or semi-rigid network is called a *gel*, liquids in a gas are *aerosols*, gases in liquids are *foams*, solids in liquids are *sols*. Note that immiscibility of liquid phases or solid phases can yield a colloid as well such as in the case of liquid in liquid to form an *emulsion* or a solid in solid to form a *solid sol*. In ceramics processing, colloidal behavior of a system directly affects a final product's properties by controlling packing efficiencies and microstructural uniformities. Mechanical properties of ceramics such as fracture toughness are directly related to structural inhomogeneities which can act as stress concentrators, and as such, control of how particles and surfaces interact at close distances is extremely important.

It is important to note that at times attractive forces might be desired. For instance, filtration efficiencies can be increased if particulates are attractive and adhere to the fibers rather than exhibit neither attractive nor repulsive interactions. Furthermore, in cases where sedimentation is desired such as in wastewater treatment, some level of attractive forces is required to promote the phase separation and leading to the formation of a sludge.

The size scale of colloids are often on the order of nanometers to microns where stability of the system can be maintained by Brownian motion of the dispersed phase in

media that allows for significant mobility or that there is a long-term kinetic limitation for separation of the phases such as in solid sols. If the dispersed phases are too large, gravitational effects can cause separation and result in colloidal instability. Furthermore, the presence of naturally occurring attractive forces between two similar bodies must be counteracted when desiring a fluidized bed. The source of this attractive force will be discussed as well as other forces which might be experienced by a particle in a colloidal system.

Forces Experienced by Particles

Force is a vector, so it contains a magnitude as well as a direction. The typical interaction of interfaces can be characterized as attractive, repulsive, or neither based on the direction of the force. When the direction of the force draws one body to another, i.e. attractive, the interaction is defined to be in the negative direction. When the force is such that the force acts to separate surfaces, i.e. repulsive, this is established as in the positive direction. Finally, when there's neither an attractive nor a repulsive force, then the two surfaces do not interact at a distance.

Van der Waals Force

All atoms and molecules exhibit attractive interactions with like species. This is termed the van der Waals (vdW) force and stems from the dynamics of electronic states of a particular species and its effect on the species around it. J. D. van der Waals was the first to consider the attraction between molecules to explain the deviations real gases have from the ideal gas law $PV = n R T$, where P is pressure, V is the molar volume, R is the gas constant, T is the temperature, and n is the number of moles. The correction for real gas behavior includes a term to decrease the ideal gas volume by a parameter corresponding to the finite size of molecules and another term to increase

the pressure to account for attractive intermolecular forces, i.e. inelastic interactions of molecules during collisions.

Three different mechanisms contribute to the total vdW interaction:[5]

1. Systems having permanent dipoles, e.g. in ionic bonding cases which result in a molecule having an effective positive charge at one terminal and an effective negative charge at the other terminal separated by some small distance. These are termed *Keesom* forces or '*orientation*' forces. An example is the attraction of NO_2 gas molecules on one another which leads to attractive force interactions. Note that there is a distinction between Keesom forces which exhibit interaction energies inversely proportional to the distance to the 6^{th} power and hydrogen bonding which is roughly inversely proportional to the distance squared.

2. Systems comprising of multiple species one of which has a dipole and the other being a non-polar, but polarizable atom or molecule can exhibit attractive interactions as well. This occurs by the interaction of the electric field emanating from the polar molecule to induce charge separation by the other species. The now induced-dipole interacts with the polar molecule. This process is termed the Debye interaction or Dipole-induced dipole forces.

3. The final mechanism applies to non-polar atoms or molecules which can have momentary/instantaneous non-uniform charge gradients due to the natural motions of electrons. This instantaneous charge separation results in an electric field which can subsequently polarize the electron distributions of nearby non-polar entities leading to attractive interactions. This is termed *dispersion* or *London* force interactions.

These force interactions can be calculated knowing an atom or molecule's dipole moment and its corresponding partner's polarizability. As applied to molecules and atoms, all vdW contributing forces exhibit interactions that diminish in magnitude with inverse distance to the power of 7, i.e. $F = C/x^7$, with F being force, x is the separation distance, and C is a constant comprising the sum of each of the three vdW components. Dispersion forces, though, play a role in all systems and are often the most dominant. The exception to this is for very small molecules or for interactions between highly polar molecules such as water interacting with a like molecule across a vacuum. In which case, the dispersion component represents only ~25% of the vdW interaction.[6]

In 1937, Hamaker was able to extend the results for vdW interactions among atoms and molecules to macroscopic bodies such as particles and surfaces by using pair-wise additivity of the interactions over all the atoms of the two entities.[7,8] The interaction potential, V_{vdW}, relationship is shown below.

$$V_{vdW} = \int -\frac{C}{x^6} \rho_1 \rho_2 dv_1 dv_2 \tag{2-1}$$

where *v* is the volume of each body, ρ represents the numbers of molecules per unit volume of each body, C is an interaction coefficient, and *x* is the separation distance. This equation can be separated into a materials term and a geometric term:

$$V_{vdW} = -\frac{A}{\pi^2} \int \frac{dv_1 dv_2}{x^6} \tag{2-2}$$

where A is a materials-specific constant termed the Hamaker coefficient equivalent to $C\pi^2\rho_1\rho_2$. Note also that force, F_{vdW}, and interaction potential are related as follows:

$$F_{vdW} = -\frac{dV_{vdW}}{dx} \tag{2-3}$$

For simple geometries pertaining to this work, the geometric results of vdW interactions are shown in Table 2-1.

The equations are seemingly rather simple, however, the difficulty lies in determining the materials' interaction or Hamaker coefficient and how to compensate for an intervening medium since the theory presented above examines the interaction in air or in a vacuum. An intervening medium always leads to a reduction in attractive force, and this will be addressed in the following chapter. The important part of this section is the understanding that vdW forces tend to contribute to materials' attraction to one another and that the interaction mechanism applies to any and all materials.

Double Layer Effects and Forces

In liquid media, often times, adsorption of ions from solution occurs giving rise to surface charges. These ions exist due to a variety of sources including acidic or basic conditions or from the dissociation of salts in a polar liquid. Oxides usually exhibit hydrated surfaces due to any presence of humidity or due to an aqueous environment. In aqueous conditions, an acidic condition often yields the adsorption of H^+ ions, giving rise to positive surface charges whereas in basic conditions, dissociation of H^+ ions or adsorption of OH^- ions give rise to negative charges. One might think that the negative charges would naturally lead to Coulombic repulsion between particles of like charges, but the reality is that they actually are brought towards one another due to oppositely charged counter ions in the intervening liquid medium.

Since the entire particle-liquid system must remain neutral, counter ions exist in solution to compensate for the surface charge. This leads to the presence of an electric double layer. The first layer called the *Stern layer* consists of transiently adsorbed surface ions held both by Coulombic attraction and van der Waals forces, while the second, termed the *Gouy-Chapman layer*, consists of a thermally-induced diffuse layer of counter ions that extend into the solution.

In liquid systems, two like particles nearing experience repulsive interactions. As the double layer overlaps, the counter ions become concentrated leading to osmotic or entropy-based repulsion by the intervening liquid.

In aqueous media, controlling the electrostatic interactions is the most common form of facilitating or tailoring a desired attractive or repulsive interaction using electrostatics. For many oxides, the hydrated surface species are directly affected by the liquid environmental conditions. For instance, the concentration of H^+ or OH^- ions in

solution directly determines the surface charge of many oxides. These species are termed potential-determining ions, and depending on their concentration, i.e. pH of the aqueous solution, the particle surface may exhibit the gamut of surface charge/potential going from positive through null to negative values. At potentials with magnitudes larger than thermal kinetic energy (kT motion), the electrostatic repulsion can keep particles separated enough to prevent aggregation or flocculation, and thus enhance the stability of most colloidal systems.

Furthermore, systems can be coagulated by modifying the electrostatic phenomena. There are three different methods of inducing coagulation or enhancing attractive interactions between particles,[9] aside from changing the pH to the so-called isoelectric point to induce a weakly electrostatic-stabilized system (which often is difficult to accomplish requiring large amounts of highly acidic or basic aqueous additions) or precipitation of salts or implementation of bridging polymers: (i) introducing nonpotential determining or indifferent ions to collapse the double layer (ii) introducing complex surface ions species which adsorb to and chelate the particles diminishing the overall surface potential and resulting in decreasing the strength of the diffuse layer and (iii) the use of heterogeneous particulate systems which exhibit counter charged surfaces which can coagulate the system. The pertinent system often involves mechanism (i) since this directly causes increased concentrations of ions in solution decreasing the osmotic pressure when double layers overlap. Increasing the concentration of a simple salt such as sodium chloride or potassium chloride by a magnitude can drastically decrease electrostatic interactions and effectively allow for the characterization of other forces of a system. Van der Waals forces don’t vary much

depending on electrolyte or salt concentration or pH, so the addition of small amounts of salt can screen for the double layer repulsion effects. Salt serves to only affect the zero-frequency contribution of the Hamaker coefficient since the electrolyte ions cannot respond fast enough or polarize at higher frequencies, therefore the dispersion force still persists even in salt conditions up through 0.1 M NaCl.[5]

When electrostatic interactions dominate a system, the force interactions are characterized by an exponential decay. The counter ions exhibit a Boltzmann's distribution of

$$\rho = \rho_0 \exp\left(-\frac{ze\psi}{kT}\right) \tag{2-4}$$

where ρ is the number density of ions with a valence of z with ρ_0 being defined as the density in the bulk solution, e is the charge of an electron, and Ψ is the electrostatic potential at some distance x from the surface and k is the Boltzmann's constant and T is temperature.

Combined with the Poisson's equation describing the net excess charge density at x, the Poisson-Boltzmann equation is obtained:

$$ze\rho = -\varepsilon\varepsilon_0\left(\frac{d^2\psi}{dx^2}\right) \tag{2-5}$$

where ε and ε_0 are the relative permittivity and the permittivity of free space, respectively. This equation can be solved with boundary conditions to give the potential (Ψ), electric field (E = dΨ/dx) and counter ion density (ρ) at any point x:

$$\left(\frac{d^2\psi}{dx^2}\right) = \frac{-ze\rho}{\varepsilon\varepsilon_0} = -\left(\frac{ze\rho_0}{\varepsilon\varepsilon_0}\right)\exp\left(-\frac{ze\psi}{kT}\right) \tag{2-6}$$

The boundary conditions being that at the midplane distance, between two charged surfaces, the field $E_0 = (d\Psi/dx)_0 = 0$, and furthermore that the electroneutrality conditions hold whereby the total charge of the counter ion in between two surfaces must be equal in magnitude and opposite in direction to the surface charges, resulting in the field at the surface E_s being related to the charge density, σ, by the following:.

$$E_s = \frac{\sigma}{\varepsilon\varepsilon_0} \tag{2-7}$$

There are a limited number of conditions where the Poisson-Boltzmann equation yields simple solutions, however, when conditions exist such that surface potentials are < 26 mV (or much smaller than the kT interaction), the charge density can be represented as a Taylor series. Furthermore, with higher order terms being negligible and the zeroth order term going to zero due to electroneutrality, a simple exponential decay representation of the surface potential can be expressed:

$$\psi = \psi_0 \exp(-\kappa x) \tag{2-8}$$

where κ is the Debye-Hückel parameter. This parameter is also the reciprocal of the so-called Debye screening length which describes the characteristic surface potential decay length and depends on the valency and concentration of the electrolytes.

$$\kappa^{-1} = \sqrt{\frac{\varepsilon_r \varepsilon_0 k_B T}{\sum_i (z_i e)^2 c_i^0}} \tag{2-9}$$

where ε_r is the dielectric constant of the liquid media, ε_0 is the permittivity, k_B is Boltzmann's constant, T is temperature, z is valency, e is the charge of an electron, and c^0 represents the bulk concentration for species i.

Based on this equation, we can see that at a specific temperature the valency is the dominant factor compared to the electrolyte concentration. Furthermore, for the case of symmetric electrolytes at room temperature, the Debye length can be easily calculated using the following expression where c^0 is the electrolyte bulk concentration in molars.

$$\kappa^{-1} = \frac{0.304nm}{z\sqrt{c^0[M]}} \tag{2-10}$$

Differentiating the potential equation and multiplying by -1 results in the force term which has the same decay relationship. Since the relationship depends on the Debye screening length, the increase of electrolyte concentration or valency resulting in increasing κ can decrease the repulsion between surfaces. Also, due to the exponential dependence of the resulting force equation, the dominance of this interaction can be determined by a linear trend observed when plotting force interactions on a log force-distance graph.

$$F_{EDL} \propto \kappa^{-1} \exp(-\kappa x) \tag{2-11}$$

DLVO Theory

The quantitative theory of colloidal stability accounting for electric double layer repulsion and vdW attraction is termed the DLVO theory for its founders: Derjaguin and Landau, Verwey and Overbeek. Similar to the Lennard-Jones potentials which are used to often describe the interaction of molecules and atoms, the attractive vdW potential exhibits a distance to the -6th dependence and is balanced by a repulsive term having a distance to the -12th dependence. The DLVO theory accounts for the vdW interaction and that of the double layer repulsion between two surfaces and can be expressed as

$$\psi_{DLVO}(x) = \psi_{vdW}(x) + \psi_{EDL}(x) \quad (2\text{-}12)$$

Overall, since the vdW force exhibits a power law interaction, it exceeds the exponential double-layer repulsion forces as the distance approaches contact. More specifically, the interactions can be divided into various phenomena depending on the strength of the interaction. In Figure 2-1,[1] the behavior at A is indicative of a vdW dominated interaction where a particle system is drawn to a minimum energy well which results in the coagulation of the system and the formation of difficult-to-separate aggregates. Increasing repulsive potentials results in the formation of a shallow well in the potential-distance plot which corresponds to the formation of weakly held flocs which, through kT energy can be easily broken up. The addition of energy through heating can cause the particles to overcome the energy barrier to coagulate. Further increasing of the repulsive interactions leads to the formation of a system with no secondary minimum and a high energy barrier for coagulation, this is usually indicative of a well dispersed and stable colloid. Finally, in D, the system is dominated by repulsive interactions which might seem beneficial at first for the stability of the system, however, the pronounced repulsive interactions means that there are limitations to how concentrated the particle dispersion can be. Increasing the concentration of salt can decrease the repulsive potential. Though, the addition of salt may be limited based on the liquid medium being used.

Non-DLVO Forces

Other interactions beyond EDL and vdW exist and come into significant play when the underlying assumptions of the DLVO theory are not met. These assumptions include, among others, that the interacting surfaces be solid and smooth and that the

intervening fluid exhibits bulk liquid properties up to the interfaces and are uniform density and orientation.[10] These so called “non-DLVO” forces can be categorized into attractive or repulsive interactions and are often termed structural forces since they relate to the structure of the surface as well as the molecular structure of the liquid media which is capable of assuming ordered structures during confinement. Many reviews exist to detail these forces including their treatment and interpretation focusing on such interactions as hydrophobic forces, hydration pressures, non-charge transfer Lewis acid-base interactions, solvation effects, and other such contributions to the disjoining pressure.[10-16]

In solution, attractive contributions beyond DLVO forces include the hydrophobic, ion-correlation, solvation, and specific binding forces. Hydrophobic forces are long-ranged attractive forces whose origins are due to molecular rearrangement due to electrostatic interactions between hydrophilic surfaces for physisorbed surfactant surfaces or due to nanobubbles upon silanated surfaces.[14]

Silica has been shown to exhibit some unique interactions which are not DLVO in nature and are different from other oxide systems. Decreasing magnitude of non-DLVO forces with increasing electrolyte concentrations beyond the DLVO regime have been observed for silica systems.[17-19] Furthermore, the presence of silica independent of surface treatment is believed to induce non-DLVO forces. One theory of the origin of this non-DLVO force and which leads to predictive capabilities and repulsive interactions is the notion of a swelled gel layer on surfaces of silica.[11,20]

The Derjaguin approximation used to relate the geometric effects of two interacting surfaces is limited to systems where the effects of particle curvature are minimal, i.e.

large particles and situations where the interaction distances are less than the radii of surfaces, which makes the effects of nanoscale roughnesses difficult to assess.[5,21,22] The use of the surface element integration technique has been used to address the role of roughness in force interactions of surfaces.[23] Through this approach, roughness or nano-protrusions could enhance adhesion, but under high electrolyte concentrations, nano-pits may actually prevent adhesive contact.[24,25] The latter result agrees well with experiments of ZnS particles.[26] Furthermore, extended DLVO interactions including vdW, Lewis acid-base, and EDL interactions were found to be reduced with increasing roughness due to particle-substrate separation distances being increased.[27] This technique is important to use and increases the accuracy of calculations and predictions especially when involving nanoparticle systems and surfaces with nanoscale roughnesses. With larger particle sizes, the Derjaguin approximation is adequate.

Methods of Stabilization

In general, there are three ways to stabilize colloid systems.[1] The first addressed previously is through electric double layer stabilization which often occurs in aqueous media where particle surfaces can exhibit surface charges. This method of stabilization might not be effective with other liquids in which particle charging is negligible. Furthermore, in aqueous systems, adjusting pH might lead to degradation of the particles or form a corrosive environment. The next and most often used method of stabilization is through the use of nonionic polymer molecules which results in two mechanisms of stabilization. The first mechanism occurs when polymers adsorb or anchor to particle surfaces, the organic chain then sterically or entropically hinders the approach by another particle with adsorbed organics on its surface. The second mechanism results from free polymers in solution, and in order for particles to near one

another, work must be done to demix the polymer from the liquid solvent in between the two particles. Finally, the third method of stabilization is a combination of the previous two in the form of polyelectrolytes. The polymer-stabilization route has a lot of benefits where specialty dispersants can be designed and tested for particular applications. However, their removal later on in the processing results in greenhouse and other environmentally unfriendly gases being produced. To foster greener processing techniques, liquids-based systems without added long-chain organics are desired. Since non-aqueous liquids are rather expensive compared to water, it becomes necessary to use predictive methods in order to limit selection to a manageable few choice systems. Furthermore, being able to characterize the change in surface interactions between two surfaces becomes much more important so that theory can further be used to select or design liquid media of interest.

Measurement of Surface Forces

Traditionally, surface force interactions of particles against particles have been indirectly examined through the use of using rheology,[28] sedimentation studies,[29] zeta potential measurements,[30-33] or using light scattering techniques to identify agglomerate sizes.[34] These techniques provide for macroscopic phenomenological approaches which use the theory of intermolecular interactions to explain observed changes in viscosity, time of agglomeration, mobility of particle systems, or agglomerate sizes in fluids. Particle-wall interaction measurements have often focused on methods to quantify adhesive forces of entrained particles on a surface by counteracting the adhesion with various methods such as centrifugal,[35] airflow,[36,37] or vibrational.[38] These techniques are useful in examining many particles at a time, but might not provide detailed forces of attraction which occur on finer nanoscale separations.

Diverse methods exist to directly quantify surface forces at very close ranges. Craig traces the historical development of indirect or direct surface force measuring instruments and techniques.[39] Some of these will be quickly highlighted here.

Attempts to measure the forces between two surfaces stretch back to Tomlinson in 1928 who sought to determine the adhesive forces between fibers or spheres of glass by measuring the separation distance to which fibers jumped when separated.[40] Rayleigh in 1937 was the first to measure both the force and separation distance at the same time by using interference of glass fringes when using a known weight to separate two surfaces of glasses from one another.[41] By 1954, Derjaguin was using a spring or cantilever balance to determine forces and then furthermore couple a force feedback solenoid into the spring to compensate for the deflection.[42] Based on the feedback response and proper calibration, the force can be determined between 700 – 100 nm. White light interferometry wasn't implemented until Tabor and Winterton in 1968 to bring the separation control down to 0.8 nm using piezoelectric transducers and measure vdW forces down to 5 nm.[43,44] Israelachvili and Tabor, in 1972, measured the force law between 10 and 12- nm for mica surfaces utilizing a similar system.[45,46] Dynamic methods exist as well which involve induced oscillations by one cantilever of material on another,[47] but this is beyond the scope of this thesis.

All of these techniques sought to determine the vdW interaction between two surfaces in air or in vacuum. The complications of measuring DLVO forces were due to the need for uncontaminated liquid environments as well as the ability to determine separations in a liquid environment. It wasn't until 1964 that DLVO forces were first investigated directly by Derjaguin et al. through measuring the interaction of crossed

platinum rods in salt solutions using photocells and a modified spring balance setup mentioned earlier.[48] The limitations of all these systems was that they weren't able to directly determine the spring deflection, just the surface separation when jump-in contact occurred, the frequency response of an oscillator, or an absolute value of surface separation.

In 1978, Israelachvili and Adams produced the surface force apparatus (SFA) developing from the previous designs by Tabor, Winterton, and Israelachvili. This device continued to measure the separation using white light interferometry but also incorporated a piezoelectric tube to determine the magnitude of spring deflections with surface separation. Furthermore, the piezo could be used to control surface separations on the order of 0.1 nm. The system has been modified many times in the past years but the same principle remains. The SFA remains one of the most used methods to measure force interactions to this day.

With the SFA, macroscopic and molecularly smooth mica sheets and other ideal materials were used to determine the interactions between surfaces through geometric reasoning that two crossed cylinders can be used to represent the interactions between a particle and an infinite plate. The sphere exhibits mathematical equivalence to the geometric mean radius of the cylinders. The atomic force microscope was developed in 1987 and incorporated similar piezoelectric tubes as the SFA, but further allowed forces between a fine tip and a surface to be measured.[49,50] The drawback to using the AFM is that the absolute distance between sample and tip are unknown and the absolute tip interaction geometry, until recently, had also been unknown.[5] The benefits of AFM is that the tip can measure interactions down to 10^{-10} N whereas the SFA can only

measure down to 10^{-8} N. Furthermore, the AFM allows for the interactions of real world components to be measured and the instrument is more widely available than the specialized SFA systems.

Atomic Force Microscopy Colloid Probe

The modern day AFM utilizes tiny probes or chips made of silicon or silicon nitride. During semiconductor processing, the chips are manufactured with cantilevers of various geometries on the ends of the chips. Furthermore, the cantilevers themselves either have tips or are tipless. Though both tip and tipless cantilevers can be modified, the tipped cantilevers are usually used for topographic measurements since the tips can be etched to yield atomically sharp structures, while the tipless cantilevers are modified by adhering materials and structures of interest such as a colloid sphere.

The AFM colloidal probe technique allows the surface interactions between different materials to be directly measured directly.[51] Briefly, a particle of one material is adhered to a cantilever tip and precisely brought into contact with a fixed surface of another material. As the two objects interact, the cantilever experiences a deflection either towards the surface or away depending on attractive or repulsive forces, respectively. These movements are accentuated by the deflection of a laser off the back of the cantilever and measured quantitatively by a series of photodetectors. The cantilever mount can be placed within a liquid cell and used to measure interactions in liquids.[52] Using colloid probes, the force interactions between particle and surface can be measured and further compared with theoretical calculations of electric double layer, vdW, as well as other forces in regards to relatively simple geometries such as spheres, rods, and flat surfaces.

Furthermore, if theory isn't present to describe the interactions, the measured interactions using the AFM are still useful as they represent real world interactions of the selected materials and can further be used to carry out experimentation and developing liquids which minimize or maximize attractive or repulsive interactions.

Table 2-1. Interaction and force equations. Equations of vdW interaction potential energy and force for macroscopic systems are shown for two geometrics of interest. R is the radius of the sphere and x represents the separation distance between the geometries.

Geometry	Interaction potential (V_{vdw})	Force interaction (F_{vdw})
Sphere-sphere	$-\frac{AR}{12x}$	$-\frac{AR}{12x^2}$
Sphere-plate	$-\frac{AR}{6x}$	$-\frac{AR}{6x^2}$

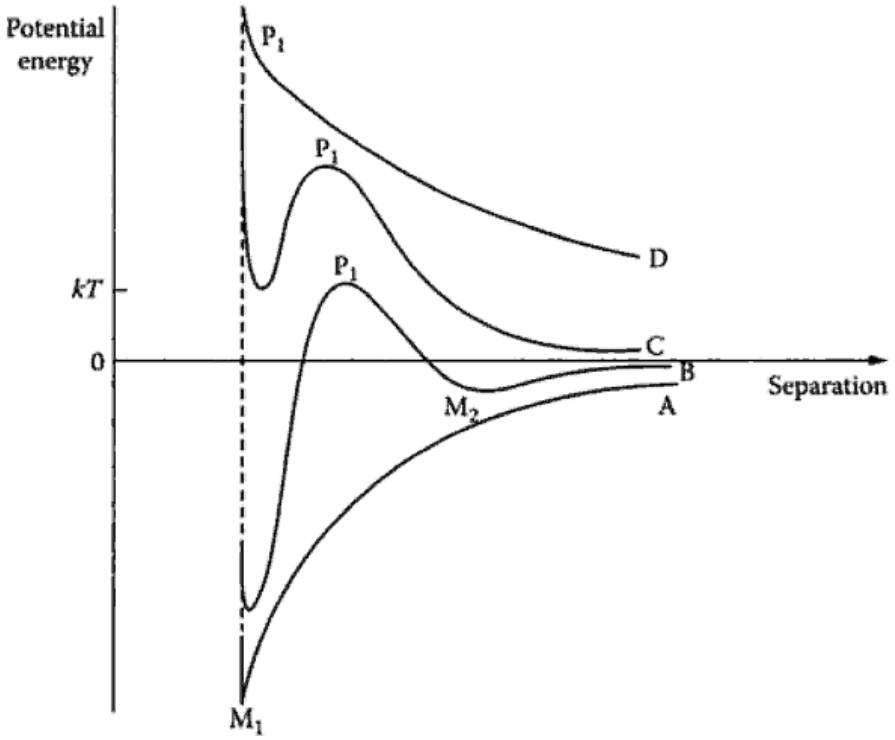

Figure 2-1. Various DLVO forces. DLVO forces depend on the dominance of electric double layer repulsion or attractive vdW interaction.[1]

CHAPTER 3
DETERMINING VAN DER WAALS INTERACTION AND SURFACE PROPERTIES

Introduction to the Hamaker Coefficient

The first step to tailoring surface forces is to use prevailing theories to facilitate the experimental design. As mentioned in the background, the vdW interaction is pervasive for all systems and is a significant contributor towards attractive interactions even at large distances. For a particular geometry, the vdW interaction potential or force depends on three things: the distance between two objects, the size of the objects, and finally, a materials-and-systems-dependent coefficient termed the Hamaker coefficient, A.

From the treatment by Lifshitz,[53] the Hamaker coefficient is a term describing the polarization dependence of each of the materials on one another- particle, substrate and intervening medium. The parameter is a difficult term to evaluate since it requires the dielectric response, ε, behavior of a material across the entire electromagnetic frequency spectrum. Parsegian and Ninham were able to provide a simplification of the dielectric response by establishing that the primary contributions to the term arise from the relaxations occurring at microwave, infrared, and ultraviolet frequencies.[54] The Hamaker coefficient term can be represented as the Ninham-Parsegian oscillator model:[55]

$$A_{\mathrm{Ham}} = \frac{3kT}{2} \sum_{\mathrm{SamplingFrequencies}} \left(\frac{\varepsilon_{A1}(i\xi_n) - \varepsilon_m(i\xi_n)}{\varepsilon_{A1}(i\xi_n) + \varepsilon_m(i\xi_n)} \right) \left(\frac{\varepsilon_{B1}(i\xi_n) - \varepsilon_m(i\xi_n)}{\varepsilon_{B1}(i\xi_n) + \varepsilon_m(i\xi_n)} \right) \mathrm{Rel}(l) \qquad (3\text{-}1)$$

where k is Boltzmann's constant, T is temperature in Kelvin, ε are dielectric responses for bodies A1 and B1 through medium m, and Rel(l) deals with the relativistic or retardation term. iξ represents the following eigen or "Matsubara" frequencies:

$$\xi_n = \frac{4\pi^2 kT}{h} n \tag{3-2}$$

where n is an integer, k is Boltzmann's constant, T is temperature in Kelvin, and h is Planck's constant. Note that the n = 0 term provides only a half contribution to the Hamaker coefficient.

The imaginary frequencies are convenient in that measured responses at real frequency values exhibit large variations near resonance during absorption phenomena. Transforming the system to exponential-based imaginary frequencies allows the responses to exhibit behavior characterized by smooth decays.

Simplifications to Determine Dielectric Response Function

The Ninham-Parsegian oscillator model was simplified by Hough and White who demonstrated that the dielectric response functions for non-conductors can be estimated from the IR and UV contribution and allows for an order-of-magnitude estimation from limited spectral data.[56]

$$\varepsilon(i\xi_n) = 1 + \frac{C_{IR}}{1 + \left(\frac{\xi_n}{\omega_{IR}}\right)^2} + \frac{C_{UV}}{1 + \left(\frac{\xi_n}{\omega_{UV}}\right)^2} \tag{3-3}$$

where C_{IR} and C_{UV} are the absorption strengths in the IR and UV region, and ω_{IR} and ω_{UV} are the corresponding characteristic absorption frequencies for the IR and UV region. If unknown, the absorption strengths can be estimated by the following relationships:

$$C_{IR} = \varepsilon_0 - n^2 \tag{3-4}$$

$$C_{UV} = n^2 - 1 \tag{3-5}$$

where ε_0 is the dielectric constant and *n* is the refractive index. Furthermore, if spectral information is unavailable, using a single UV term equation might be sufficient to provide a rough estimate on dielectric response where the C_{UV} is approximated by n^2-1 and ω_{UV} by the first ionization potential in electron volts divided by the reduced Planck constant, also called Dirac constant or h-bar.[55]

Returning to the determination of the Hamaker coefficients, Parsegian provides a sample MathCAD program to determine the vdW interaction of water across a hydrocarbon film.[55] The program was modified for geometry and for simplification.

Repulsive Van Der Waals Forces

Of particular interest experimentally and scientifically is when the Hamaker coefficient is negative, which results in a condition of “destructive electrodynamics” and repulsive vdW force interactions between two materials.[57] Based on the difference parameters expressed in equation 3-1, this scenario occurs when the dielectric permittivity or response of the medium is in between the responses of the two materials. Thus, immediately, it can be shown for a limiting case when two bodies are the same, there can only be attractive vdW interactions; or in a condition where the medium exhibits similar dielectric response as the body, there can be a condition of no interactions.

Repulsive vdW forces often occur in solid-liquid-air interface conditions and have been used to describe the wetting properties of liquid helium in 1961[58] and that of pentane wetting and spreading on the surfaces of water.[5] Repulsive vdW were later used to describe the presence of a wetting hydrocarbon film on the order of 20 – 80 nm in thickness which opposes a gas bubble being pressed onto an alumina or other hydrophilic surface.[59,60] Measurement of the hydrocarbon thickness incorporating the

Hamaker coefficient was found to be in good agreement with the disjoining pressure upon the film. Furthermore, van Oss estimated the Hamaker coefficients for various polymer pairs in solvents, and determined that when the coefficient was greater than 0.03×10^{-20} J, the polymers would be miscible, and if the coefficient was less than -0.03×10^{-20} J, the polymer pair would be immiscible and phase separate.[61]

Direct measurement of repulsive vdW forces of two condensed phase separated by a solvent medium weren't made until late 1990s due to the rarity of solvent and materials combinations which would yield such conditions. Milling et al were the first to measure repulsive vdW forces using an AFM for system consisting of 20 - 40 nm thick gold coated tungsten spheres against polytetrafluoroethylene (PTFE) in the presence of low-polarity solvents such as cyclohexane, dodecane, p-xylene, and bromobenzene and polar solvents such as dimethyl formamide.[62] The force curves were analyzed by plotting the apparent separation distance with the square-root of the term corresponding to the particle radius divided the force. A line extrapolated to the apparent separation ordinate would have a slope corresponding to the negative square root of 6 over the Hamaker coefficient. Examination of retardation effects was not necessary to yield values close to calculated Hamaker coefficients suggesting that the approximations of spectral parameters compensated for the omission. Meurk et al. measured repulsive vdW interactions between silicon nitride pyramidal tips and flat silica glass surface at a separation distance of about 2.5 nm in diiodomethane and 1-bromonaphthalene liquids.[63] Lee and Sigmund later explored these interactions with silica or alumina against PTFE in cyclohexane and found that the repulsion extends out to about 3 nm before decaying rapidly.[64,65]

Furthermore, mesocarbon microbeads for lithium-ion applications and to facilitate self-assembly of colloidal-scale devices were examined upon a variety of surfaces from indium-tin oxide, PTFE, and lithium-cobalt oxide ($LiCoO_2$) with the carbon experiencing repulsion at 4 nm. PTFE is often used as a material of choice since its strong carbon-fluorine bond leads to a very low dielectric response, and its lack of surface charging in liquids restricts its interaction to primarily those of vdW dispersion interactions.[66] The most recent explorations found that repulsive vdW leads to so-called superlubricity and extremely low friction coefficient of 0.0003 between a gold sphere and PTFE in cyclohexane.[67] Finally, Munday et al. measured repulsive vdW forces for gold spheres against a silica glass plate in bromobenzene with significant discrepancy between theory and experiment being attributed to dielectric response/optical properties uncertainties.[68] Based on the literature, the difficulty of adhering a particle to a probe tip to manufacture a colloid probe, the experimental conditions requiring stringent controls and clean and well-characterized surfaces, and the effects of non-DLVO forces are the concerns for the AFM technique and results interpretations.[69]

System of Interest

In real world processing, there are two primary interactions for fluidized particle system: internal and external. Internal interactions represent particle-particle interactions and are often the subject of colloidal textbooks. Internal forces are often difficult to probe and often require more macroscopic investigations such as using settling rates, sedimentation densities, particle size and mobility measurements to determine surface properties, etc.

External interactions refer to particle-wall interactions which often occur at the edges of a fluidized bed. Often times, it is favorable to have a minimization of attractive

external surface force interactions between the two surfaces as attraction and its eventual adhesion works against and removes energy from the mobile system. Furthermore, during molding or packing processes, attractive interactions may yield non-uniformity of surface features which will later act as stress concentrators. External interactions are especially well-suited for exploration using advancements in the atomic force colloid probe technique.

As a model system, well-characterized silica spherical particles against that of flat stainless steel surfaces are selected for investigation. A benefit of this model system is that various solvents have been used and uniform commercially available silica spheres have been developed, particularly for use in chromatography-based applications. As mentioned prior, historical development of processing has often taken a trial and error approach, and already a handful of liquid media and their effect on particle-particle interactions already exist. Understanding the particle-wall interactions for specific liquid media contributes to the body of knowledge for this system and is directly applicable for the chromatography field.

This chapter focuses on characterizing surface properties to facilitate the calculations necessary to predict surface-distance interactions in various solvents. Predictions of interaction behavior between silica and steel are presented for various liquid media and establish a basis by which to explore later on using atomic force microscopy.

Surface Properties of Silica Sphere

Zorbax silica acquired from Agilent Technologies was examined due to their mono-modal particle size of 7 μm in diameter and as part of a research project to facilitate understanding of how these particles behave in various solvents. Both

hydrophobic and hydrophilic-modified particles were acquired, but emphasis of this section is on the hydrophilic system. These particles exhibit high porosity and are used as the stationary phase in high performance liquid chromatography (HPLC) columns.

Scanning electron microscopy

Scanning electron microscopy was used to examine the surface features of the particles. Briefly, the principles of scanning electron microscopy involve the generation of an electron beam by means of thermionic emission or field emission through tungsten or LaB_6 filaments. The electron beam is rastered along and focused on the sample surfaces through the use of electromagnetic scanning coils and lenses. Two types of 'lenses' usually exist: the condenser lens which demagnifies the beam into a narrow diameter spot size and an objective lens (or final condenser lens) which is responsible for focusing the beam directly onto the sample. The interaction volume is usually in the shape of a tear drop extending into the sample for about 5 microns. Edge effects and the concentration of the interaction volume across a small region result in higher electron generation from a larger emission area and contribute to the contrast and resolution of the features. The main types of electrons used for imaging are referred to as 'secondary electrons,' which are the low kinetic energy electron produced by inelastic scattering with the primary electron beam. Using an Everhart-Thornley Detector biased positively ensures the capture of the generated electrons. Their interaction with a scintillator material which emits light when electrons collide is then detected and the contrast levels yield topographic information.

SEM microscopy was used to image the particles and quickly provide an indication of the surface morphology, see Figure 3-1. The silica spheres were adhered to carbon tape on an aluminum sample mount. Since the silica exhibits low electro-conductivity,

charging is an issue and the particles need to be carbon coated. Charging is the process where the primary electron beam causes the particle to become negatively charged due to inability to conduct the electrons away. This results in repulsion of the electron beam and poor resolution. The first image was acquired by use of a thermionic emission JEOL 6400 SEM. In this image, the pores of the spheres can be detected by the lack of well-defined edges. Higher resolution field emission SEM was used to acquire the second image. It was found that the carbon coating smoothed out the pores and enhancement of the surface topography could only be seen on dislodged samples which exhibited gradual charging. The sphere presented is partially coated along the top portion, but uncoated for the lower portion. The charging behavior here was actually used to increase the contrast of the surface topography which demonstrated the highly porous nature of the particle.

X-ray diffraction

A Philips APD 3720 powder diffractometer was used to perform X-ray diffraction (XRD) and characterize the crystallinity of the particles. Particles were adhered to a petrographic glass slide using a solution of collodion in amyl acetate. A copper K alpha source was used. Briefly, high energy electrons are accelerated and impinged upon a metal target, in this case, copper. The electrons have enough kinetic energy to dislodge a K-shell electron resulting in transitions of higher energy electrons to occupy the inner shell. This transition must necessarily result in an emission of a photon in the form of x-rays since the higher energy electron is going to a lower energy state. X-rays exhibit diffraction when interacting with crystalline lattices according to Bragg's law where when the Bragg condition is met, constructive interference results and is detected.

The XRD spectrum of the particles is shown in Figure 3-2. The particles examined were confirmed to be amorphous, and thus, properties of amorphous or glassy silica can be utilized to determine the necessary parameters to calculate the expected vdW interaction.

Surface Properties of Stainless Steel Plate

During processing, often times particles come into contact with steel components whether they are packed into chromatography columns or transported tubes or pressed by a die. A sheet of mirror-polished 316L stainless steel was purchased from McMaster-Carr (part no. 9759K11). The steel was annealed and cold finished by the manufacturer and has a thickness of 0.76 mm. The large square plate with edge length of 30.48 cm was cut into smaller 1.5 cm square edge pieces using a Dremel rotary tool with a blade designed for cutting metal. The subsequent samples were deburred and then epoxied to AFM magnetic specimen discs made of stainless steel (alloy 430).

Auger electron spectroscopy

The surface chemistry of the plate was determined by using Auger electron spectroscopy (AES). Three points on the cut plate were examined at 52 cycles of 6 second sputtering with 3 kV Ar-ion sputter. During scanning by an electron beam, inner shell electrons can be dislodged from an atom. To fill the resulting hole, a higher energy electron can lose energy and occupy the lower energy state. When the emitted photon energy interacts with another higher energy state electron, the excitation can dislodge the electron from the atom. These resulting electrons are called characteristic Auger electrons and are emitted from the surface of the material. Due to the low energy of the electron, the path length is very short and thus only surface Auger electrons at less than 10 nm make it out of the specimen.

The results are shown in Figure 3-3. The data is presented as counts over time. With each time increment, Argon ions are used to ablate the surface providing, in essence, a depth profile. However, the results are not specifically a depth profile, since the ablation is not uniform or consistent depending on the chemical composition. The counts furthermore are relative due to the variations in the number of electrons which can be emitted from each material. Instead, the profile indicates compositional changes, and to interpret the data, limited a priori knowledge of the specimen's layers needs to be known.

From literature we find that the expected structure of stainless steel layers is comprised of a contamination region of organic materials, a passivating film, and finally the bulk composition,[70] which is expected to be the standard 316 composition of Fe, <0.03% C, 16-18.5% Cr, 10-14% Ni, and 2-3% Mo but with a lower carbon content (represented by the L in 316L).

The important indication is that the surface is comprised of a chromium-rich layer. This corresponds well to literature that the chromium forms a chromium oxide layer protecting the bulk from further oxidation and corrosion. The chromium oxide passivation layer of 316L is expected to be on the order of 3-5 nm thick with mechanical polishing and can be extended to as deep as 50 nm with passivating nitric acid treatments for 60 mins.[71] We make the simple assumption that the interaction of the silica sphere is with that of the chromium oxide layers at short, sub 25 nm distances. At larger distances where the bulk becomes the dominant material, then the interaction is expected to be with the composition of the 316L bulk solution and this complicates the calculations exponentially.

Atomic force microscopy

Tapping mode AFM was used to characterize the topography of the stainless steel surface, see Figure 3-4. A scan size of 20 μm square with a slow scan rate of 1 Hz was used, corresponding to a tip velocity of 40.1 μm s^{-1}. The figure on the left represents the height data obtained by the scan and on the left is the amplitude data which provides a sharper, more contrast view of the surface. Note that we can see some regions of contamination presented as large white dots in the height images upon the surfaces. These contaminants are probably dust and other organics from the atmosphere and exhibit a height of 65 – 115 nm. Under liquid environments, these contaminants are expected to be rinsed away and shouldn't pose issues when measuring force interactions. However, to ensure contaminants aren't the cause of force interactions, multiple regions at μm distance apart should be measured.

Dielectric Response Functions

Based upon the surface chemistries of the materials system, the dielectric response functions were determined using parameters from the literature and estimations. In general, the parameters used to calculate the dielectric response function can be estimated by acquiring the frequency-dependent refractive index of the material. This is quite difficult as it requires a wide-range of characterization techniques to acquire a response for each frequency region. In the microwave region, wave guide resonance techniques are often required to extract the dielectric response and absorption. In the infrared region and the visible, Fourier transform infrared spectroscopy and refractometry are used, respectively. Finally, in the UV range, inelastic x-ray scattering spectroscopy with synchrotron x-rays can be used for a variety of solvents, especially with those having high vapor pressures.[72-75]

The dielectric response functions are presented in Figure 3-5 for the solid phases as well as for various solvents. Most of the spectral parameters were obtained largely from reports in the literature.[65,76] For some parameters of the chromium oxide and tetrahydrofuran, the absorption frequencies were estimated. The values used are presented in Table 3-1.

The corresponding calculations for the Hamaker coefficients follow. This is realized through the use of a Mathcad calculations sheet by evaluating the following expression:

$$A_{A1mB1} = \frac{3kT}{2}\left[\sum_{\text{Sampling frequencies}} D_{A1mB1}(\xi_n) + 0.5 D_{A1mB1}(0)\right] \tag{3-6}$$

where, from equation 3-1, ξ_n represents the sampling frequencies (equation 3-2), and D represents the difference over sum product for a body (A1) with another body (B1) interacting across a medium (m) with a half contribution at n = 0.

$$D_{A1mB1}(i\xi_n) = \left(\frac{\varepsilon_{A1}(i\xi_n) - \varepsilon_m(i\xi_n)}{\varepsilon_{A1}(i\xi_n) + \varepsilon_m(i\xi_n)}\right)\left(\frac{\varepsilon_{B1}(i\xi_n) - \varepsilon_m(i\xi_n)}{\varepsilon_{B1}(i\xi_n) + \varepsilon_m(i\xi_n)}\right) \tag{3-7}$$

In the calculations, n was assumed to go from 1 to 1000, providing a range of frequencies from 2.468×10^{14} to 2.468×10^{17} radians per second addressing the frequencies between the infrared through the visible and into the ultraviolet. This part of the spectrum dominates the contributions to the vdW interactions. Note that the conversion from angular frequencies to frequency is completed by dividing the angular value by a factor of 2π.

Table 3-2 shows the computed Hamaker coefficients and its effect on the expected force interaction at a 10 nm distance for silica against chromium oxide in the various liquid media. At 10 nm, silica particles would experience a vdW attractive force

of 0.4 – 0.5 nN towards the steel surface in the presence of all the solvents except for THF, which exhibits a repulsive force of 0.14 nN due directly to its having a negative value of the Hamaker coefficient.

Force is graphically represented with respect to methanol in Figure 3-6. Replacing a solution of methanol with 1 or 2-propanol or with 1-butanol can decrease the force interaction at 10 nm by 11% or 12%, respectively. Furthermore, use of 2-butanol is expected to enhance the attractive force by 1.4%.

Ethanol was not included in the table nor the figure due to difficulties of finding its microwave frequency contributions in the literature which significantly impacts the calculated value. Using the Parsegian approximation which allows for determination of the UV contribution, ethanol having a refractive index of 1.359 and conversion of its first ionization potential (10.15 eV) into the characteristic absorption frequency (1.542×10^{16} rad s^{-1}) leads to a calculated Hamaker coefficient of 4.289×10^{-20} J. This coefficient is much lower than the expected value due to neglecting the contributions from the microwave and infrared domain which should be significant since the static dielectric constant minus the refractive index squared is significantly greater than zero at 20.56.[56] Comparison of the refractive index suggests that the polarization behavior of ethanol should actually be between methanol and 2-propanol, and its Hamaker coefficient for the interaction between silica and steel should actually be between 7.3 and 8.2×10^{-20} J.

Summary and Solvents of Interest

Note that for two solid phases made of the same material interacting with one another, minimization of the attractive vdW interaction is achieved by selection of a solvent medium with similar DRF as the solid phase. For the interaction of two different solid phases, and especially interesting from a scientific standpoint, is when the

dielectric response of the fluid medium is in between the responses of the two phases, such as with the case of THF whose dielectric response resides between those of silica and the chromium oxide surface layer of the steel plate. When this occurs, the Hamaker coefficient becomes a negative value, which makes the vdW force equation into a positive value corresponding to a repulsive force interaction. This would provide conditions whereby two surfaces are dispersed without surface charging mechanisms or by the use of adsorbed organic dispersants.

The solvents of interest for the silica and steel system are THF and methanol, which happen to also be the used commonly in the chromatography industry as packing solvents and rinsing solvents. Since the other alcohols for which calculations of Hamaker coefficients and force interactions don’t yield much difference compared with methanol, these two solvents will be focused on experimentally to quantify the force interactions between the two surfaces in liquid media.

Table 3-1. Parameters used to determine dielectric response functions.

Component	n_D	ε_0	C_{uv}	ω_{uv} (rad s-1)	C_{ir}	ω_{ir} (rad s-1)
Silica	1.46	3.82	1.1316	2.034E+16	0.829	8.670E+13
					0.095	1.508E+14
					0.798	2.026E+14
Chromic oxide	2.5	11.9	5.2500[b]	2.000E+16[a]	5.65[b]	1.000E+14[a]
Toluene	1.4961	2.38	1.2383	6.633E+15	0.0642	2.183E+13
					0.02295	4.485E+13
					0.0545	7.780E+11
Tetrahydrofuran	1.404	7.6	0.9712[b]	6.000E+16[a]	5.6287[b]	1.000E+15[a]
Methanol	1.3288	33.64	0.7657	9.189E+15	0.254	3.058E+13
					0.123	4.149E+13
					1.042	8.682E+13
					2.801	1.007E+14
1-Propanol	1.385	20.8	0.9182	8.970E+15	0.2134	3.148E+13
					0.1778	4.317E+13
					0.3808	8.802E+13
					0.70977	9.977E+13
2-Propanol	1.3776	20.18	0.8978	9.189E+15	0.0198	2.434E+13
					0.05927	2.842E+13
					0.1441	3.466E+13
					0.1801	4.125E+13
					0.2208	8.874E+13
					0.53462	9.917E+13
1-Butanol	1.3993	17.84	0.9580	8.761E+15	0.13545	3.178E+13
					0.13233	4.287E+13
					0.26674	8.784E+13
					0.50743	9.917E+13
2-Butanol	1.3978	17.26	0.9538	7.245E+15	0.2582	2.998E+13
					0.2185	4.113E+13
					0.4767	8.904E+13
					0.9931	1.004E+14
Benzene	1.5011	2.28	1.2533	6.776E+15	0.00969	2.015E+13
					0.00561	4.437E+13
					0.0114	9.144E+13

Table 3-2. Calculated Hamaker coefficients and expected vdW force at 10 nm for silica interacting with steel surface in various solvents assuming a particle size radius of 3.5 µm.

Solvent	Hamaker coefficient (J)	Force @ 10 nm (N)
Methanol	8.1914E-20	-4.78E-10
Toluene	7.4646E-20	-4.35E-10
THF	-2.4108E-20	1.41E-10
1-Propanol	7.2765E-20	-4.24E-10
2-Propanol	7.2668E-20	-4.24E-10
1-Butanol	7.1561E-20	-4.17E-10
2-Butanol	8.3097E-20	-4.85E-10
Benzene	7.2636E-20	-4.24E-10
Ethanol	4.2894E-20	-2.50E-10

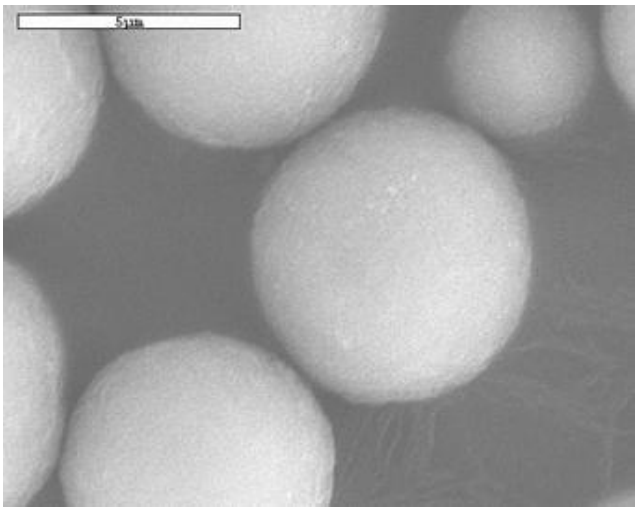
A

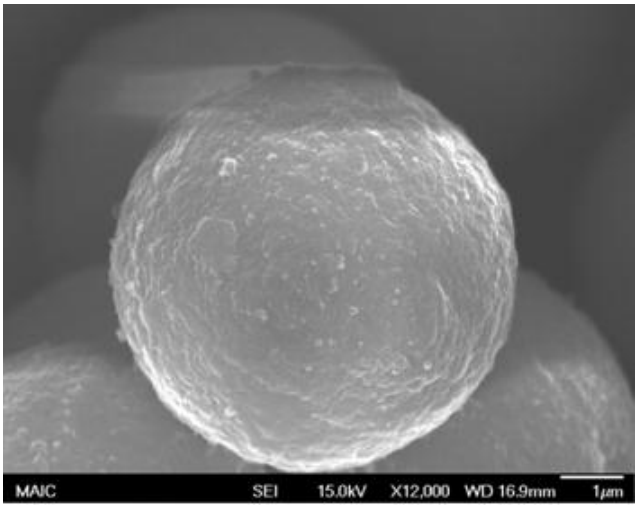

B

Figure 3-1. Electron microscopy of porous silica spheres. A) Conventional thermionic SEM image of silica particles. B) Field emission-SEM of silica particle.

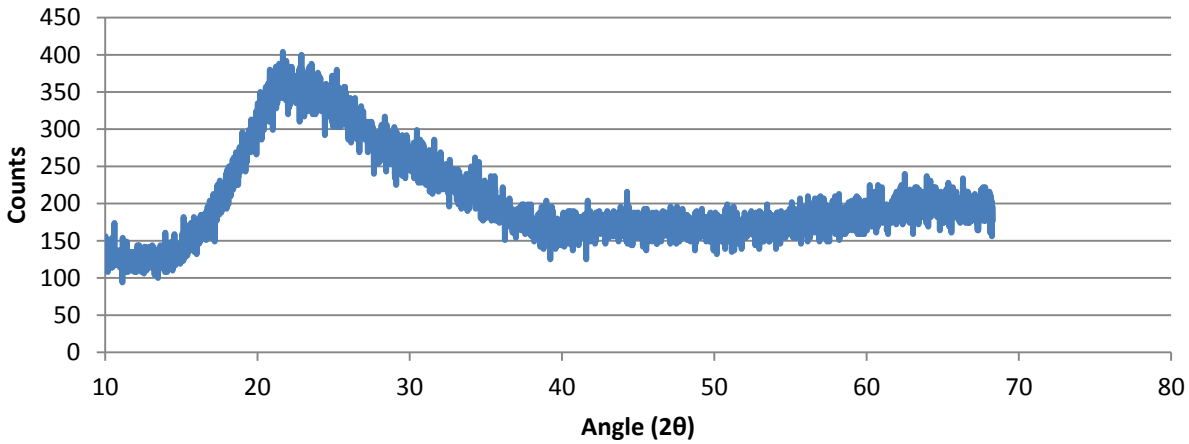

Figure 3-2. X-ray diffraction of silica particles.

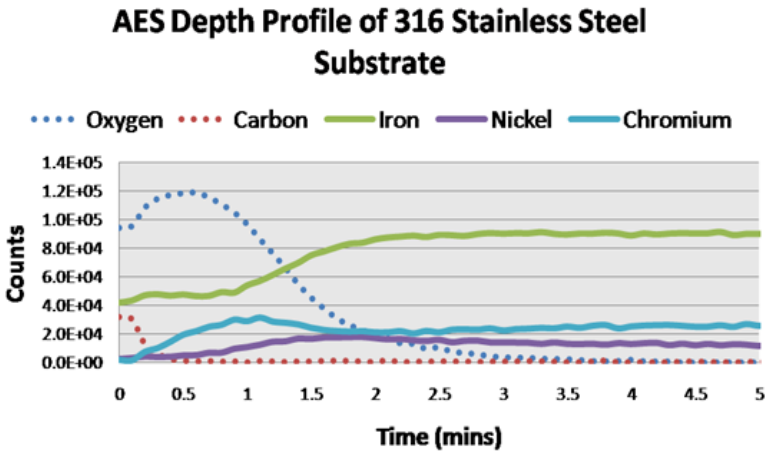

A

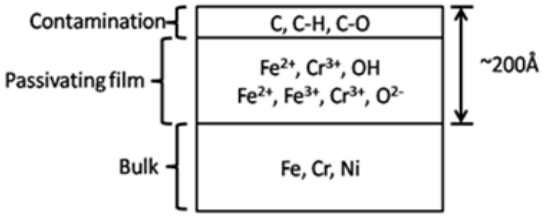

B

Figure 3-3. Auger electron spectroscopy of steel. A) Depth profile of the 316L stainless steel surface as determined by AES. B) Representation of the expected chemical constituent of the stainless steel plate.

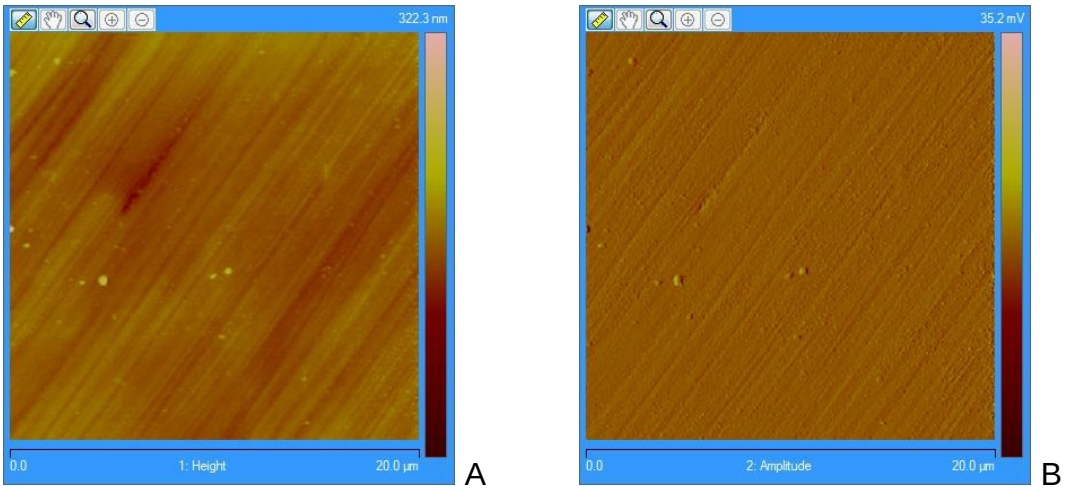

Figure 3-4. Characterization of the stainless steel plate surface using tapping mode on the Dimension 3100 AFM. A) Raw height information of surface. B) Amplitude information increasing contrast of topography features.

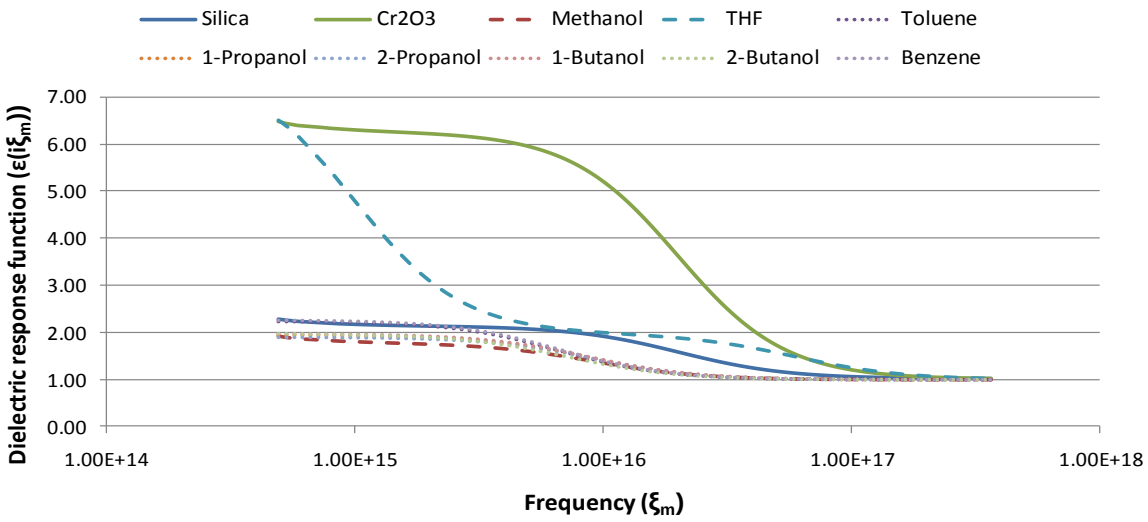

Figure 3-5. Dielectric response function calculations for the various components of the system containing silica spheres interacting with a chromium oxide passivation layer on stainless steel in various liquid media.

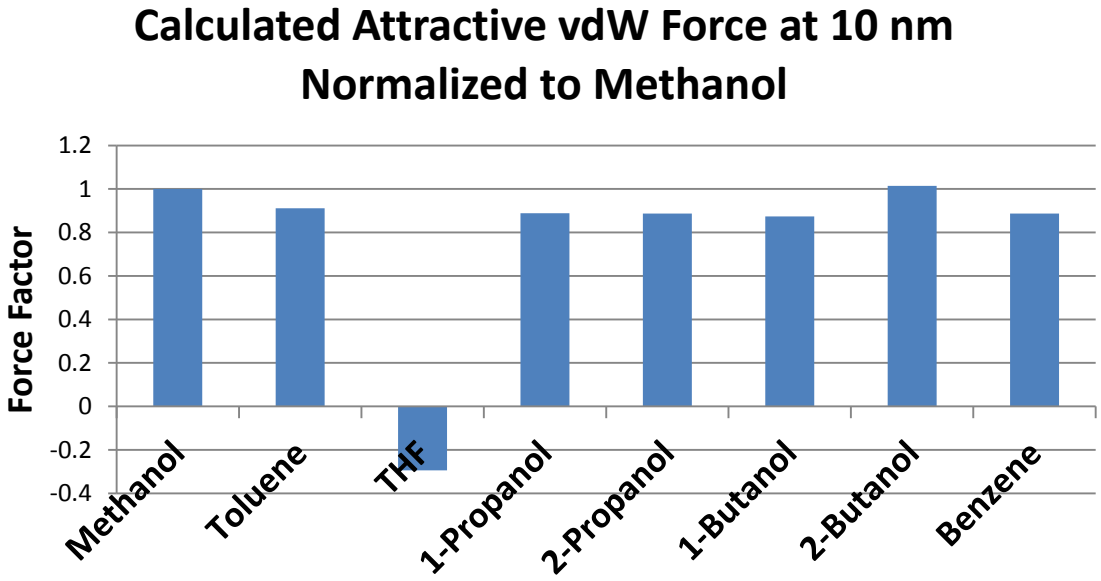

Figure 3-6. Force comparison for silica against steel surfaces in various liquid media normalized to methanol.

CHAPTER 4
IMPLEMENTING COLLOID PROBE ATOMIC FORCE MICROSCOPY

Overview

The previous sections laid out the historical developments of surface force measurements and the theoretical basis as well as provided the mathematical treatment for the interactions between a sphere and plate with an intervening medium. The results of the theoretical analysis provide some guidance into designing a solvents-based system which can be used to decrease the use of organic dispersants during processing. To accomplish this, the colloid probe technique of atomic force microscopy is employed.

Theoretically, the characterization is straight forward with a particle being attached to a cantilever having a reflective backing, resulting in a colloid probe. The new colloid probe can be inserted into the AFM just as one would with a conventional contact or tapping mode tip. A laser would then be deflected off the back of the cantilever into the set of cross photodetectors. The cantilever and detector assembly moves simultaneously, therefore if no net attraction or repulsion is experienced by the cantilever, there would be no deflection. If there is an attractive interaction, the cantilever would deflect the laser towards more negative values; likewise, if there are repulsive interactions, then the deflection would be towards a positive direction.

However, there are a number of complications and challenges that need to be addressed to successfully go from having a vial of particles to measuring its interaction against another object within a liquid medium. Firstly, the attachment of a single 7 μm diameter particle to a cantilever and ensuring adhesion is not trivial. Adhesives which can withstand a diverse set of solvents need to be utilized and care and control must be

taken to adhere one single particle onto the tip of a cantilever. Next, though the standard liquid cell is made of glass and is resistant to a wide variety of solvents, there are many polymeric components which degrade in the presence of various organic solvents. The sealing O-ring made of silicone, fluoro-silicone, or even Viton, though solvent-resistant, is not compatible with ethers such as THF. Furthermore, the silicone tubes through which the liquid medium is fed into and removed from the fluid cell is also not compatible with many solvents. Other challenges including how to determine what the actual region of interaction is of the silica particle, and furthermore how to determine the spring constant to convert deflection of the cantilever to a force equivalence need to be addressed.

The focus of this chapter is to explore in detail how to address these challenges and facilitate the acquisition of the interaction behavior without introducing artifacts. The first part of the chapter discusses the availability and functions of two different atomic force microscope setups. Next are highlights to the necessary modifications which allow a commercially available atomic force microscope system to be able to handle a variety of liquid types. This is followed by the design and construction of a colloid probe addressing particle attachment.

Atomic Force Microscopes

Two types of atomic force microscopes exist depending on the location of the piezoelectric scanner relative to the cantilever and the plate sample. The first type is a piezoelectric scanner which supports the plate sample and actually moves the sample on the x-y-z plane. The cantilever remains stationary in contact scanning mode. The longer the scanner, the greater the upper range of the scan sizes during topographic characterization. The example used here is the Nanoscope 3-controlled Multimode AFM

manufactured by Digital Instruments. The system available has two scanner units E and J, where E is a shorter scanner and J is the larger sized scanner. The shorter system has a maximum scan size range of 10 µm x 10 µm with a vertical range of 2.5 µm. The larger scanner exhibits a maximum scan size of 125 µm x 125 µm with a vertical range of 5.0 µm. There are sample limitations such as sample sizes with diameters of ~ 1 cm in diameter and having a height of less than 2 mm.

Unique cantilever tip holders are available for various applications ranging from measuring topographic variations to magnetic field or electric field variations to a self-contained liquid cell module. Of particular interest is the liquid cell module which consists of a glass housing with a wire to maintain an AFM chip. The housing is surrounded by an O-ring which when a sample is raised to the tip forms a seal allowing fluid to be supplied as well as evacuated through two ports in the glass housing. The O-ring design ensures only a small amount (~ 50 µL) of liquid is needed. Unfortunately, the small spacing required that the sample surface be relatively flat and furthermore that the O-ring could slide back and forth on the sample surface during topographic scans.

The other configuration is where the piezoelectric is connected to the cantilever which is then allowed to move to engage a stationary sample. This configuration is found on the Dimension 3100 AFM and allows for the system to accommodate much larger sizes such as 150 mm wafers since a motorized stage can coarsely position a sample into view. The maximum scan size is also on the order of 100 µm x 100 µm with a height differential of 6 µm. A series of versatile chip/tip holders also exist for this configuration.

The liquid cell is a glass cantilever tip holder attached to the underside of the piezo column. The spacing between the fluid cell and the piezo is shielded using a silicone skirt. The use of this technique depends on the ability for the fluid to bead onto the surface of the sample. Since there is no enclosure, high vapor pressure solvents cannot be used as their evaporation sets up a dynamic condition destabilizing the laser signal. Furthermore, liquids need to be able to bead onto the surface and form a fluid column encompassing the scanning region of interest and the scanning tip. This becomes difficult for situations such as imaging in alcohols which tend to wet a surface and have a high vapor pressure. In such cases, an entire sample surface and the tip holder with the protective sleeve needs to be immersed and scanned in the fluid. Evaporation of hazardous chemicals becomes a major issue. The challenges with incompatibilities with the skirt material also are present for this system.

The benefit of using the AFM 3100 is that, unlike the Nanoscope III controlled AFM Multimode system, the instrument has the capability to determine the cantilever spring constant which is required to convert cantilever deflection information to an equivalent force. However, the force interactions in the presence of high vapor pressure ethers, alcohols, and other liquids are better measured using the Multimode AFM system. Thus, both AFMs are needed to effectively provide a streamline measurement system. Note that subsequent controllers such as the Nanoscope IVa, V, and beyond can be used with the Multimode system to further facilitate an instrument set up to measure both spring constant and acquire force curve information within enclosed liquid environments.

Fluid Cell Modifications

Modifications to the liquid cell system of the multimode AFM system needed to handle a wide variety of liquids are addressed in this section. The glass fluid cell can handle various liquids and needs no direct modifications, however, the polymer parts need to be modified or replaced. Otherwise, chemical attack by the various liquids of consideration may result in their degradation and failure as well as potentially introducing artifacts into the measurements.

The silicone O-ring and tubing system was found to be compatible with water and alcohols such as ethanol, methanol, and 2-propanol. However, limited compatibility with ethers such as THF results in degradation and sealing issues. A quick experimental test was conducted to determine the effects of THF on a silicone O-ring. Within 30 minutes of immersion, the O-ring went from having a diameter of 1.1 cm to 1.6 cm. This is a length increase of 45%. Such an expansion would force the O-ring out of the glass tip holder grooves and the seal integrity would be compromised. Likewise, expansion of the silicone tubing decreases its ability to maintain a sealed environment and allows for air and bubble contamination.

Other polymeric materials were examined for compatibility (see Figure 4-1). Based upon chemical compatibility charts offered by such databases as the Parker O-ring Handbook, THF exhibits compatibility with perfluoroelastomers such as Chemraz or Kalrez as well as PTFE. However, PTFE is too rigid and does not have the elasticity to ensure proper sealing as an O-ring.

Kalrez fitting O-rings (AS-568A) were selected to be used as the sealing material. Though more rigid than a silicone O-ring, the Kalrez fitting was elastic enough to form a tight seal. Unfortunately, the fluid cell did not exhibit a groove with a standard-sized O-

ring diameter, so the ring had to be modified. Using a rotary tool and a sanding attachment, the outer edge of the O-ring was sanded down and the inner diameter was expanded to be able to fit into the groove of the fluid cell (see Figure 4-2 for similar modifications done on PTFE O-ring). The height was left unmodified allowing the O-ring to seat snugly between the fluid cell and the flat sample surface when engaged.

In this setup, one of the difficulties which might arise is the inability for multiple engagements without reseating the O-ring. When disengaging the tip from the sample, the O-ring remains recessed into the groove, and therefore the seal is lost. Minimizing the disengagement distance from the sample can maintain the integrity of the seal, but comes at the cost of increasing the risk of cantilever breakage during evacuating, rinsing, and refilling of liquid media whereby fluid could force the cantilever to collide with the sample surface with enough force to cause damage.

Since the tubing and Luer-Lok™ connectors do not need to be flexible and elastic, they were replaced with the more available and cheaper but rigid PTFE tubing. Further problems were encountered using a BD plastic syringe with a rubber plunger, where the rubber plunger would chemically weld to the wall of the plastic in the presence of the ether. This was solved by using an entirely glass micropipette with steel Luer-Lok™ connections.

Finally, one of the major concerns is the evaporation and exposure of hazardous solvents into the atmosphere. This was addressed using a containment system involving the glass syringe at the out port for drawing fluids from a glass vial at the in port (see Figure 4-3). The glass vial has a modified cap with a drilled hole just large enough for tubing to fit through to submerge into liquids of interest. Liquids may be

drawn into the cell by loosening the liquid vial cap, and then cap closed and tubes clamped to form a static liquid environment. To exchange liquids, the clamps are removed and the vial of the old liquid is removed as well. The syringe is drawn to remove as much of the used media as possible and emptied into a waste bottle. Next, the modified cap is installed onto another vial of new liquid and the syringe is reconnected. At least 10 mL of new liquid is carefully drawn (with loosened cap) through the system in 5 mL increments to dilute and rinse out any remaining former liquid, again with the glass syringe being dispensed into a waste bottle each time. The syringe is then drawn once more and clamps attached to form a new static liquid environment. This process can be repeated to exchange the liquids in the cell multiple times so long as the O-ring seal is not breached.

Colloid Probe and Particle Attachment

In order to measure the force experienced by a particle, it first needs to be attached to the tip of a reflective cantilever, whose deflection can be used to determine the force experienced by the particle. The challenges involved include isolating and manipulating single sub 10 μm-sized particles, adhering the particle onto a cantilever, and devising methods to clean the cantilever prior to experimentation to remove any contaminants which might have settled onto its surfaces.

Colloid probes were manufactured utilizing an in-house system consisting of a microscope and micromanipulators. The microscope used was a Carl Zeiss Axiovert 100 inverted microscope with a metallic stage. A set of two micromanipulators (OptoSigma MB-L-65C-UNC) with magnetic bases was attached to the metallic surface. Furthermore, a set of removable alligator clips which could be mounted into the micromanipulators were used to hold various components requiring fine manipulation.

A protocol was developed to ensure particle attachment occurred consistently and efficiently. First, one or two particles need to be isolated. This is accomplished by dipping a syringe needle into a collection of silica particles which results in the accumulation of a mass of particles at the tip. Next, it's mounted to the micromanipulator using an alligator clip and the syringe tip is brought into focus in the microscope. Another clean syringe needle is mounted to the other micromanipulator using the other alligator clip. This is then manipulated to bring into same focal plane of the previous needle. Now that the two tips are along the same plane, the clean tip can be brought close enough to collect a particle or two to the needle. This is set aside for later attachment.

Next, a new syringe needle is used to collect a bead of mixed epoxy and resin or other adhesive. Similar to the previous step of acquiring a single particle, the same procedure is followed to acquire a small sliver of the adhesive onto the tip of a syringe needle.

Leaving the tip with the adhesive on the tip in focus, the cantilever is mounted into the other micromanipulator and manipulated until the tip is brought into focus. Focusing edge to edge and noting the angle difference allows the center point of the cantilever to be found. Using a tipped cantilever allows for the center point to be easily determined. Once the center point is in focus, the syringe needle with the adhesive tip is brought to place a tiny droplet of epoxy unto the cantilever.

The glue syringe is removed, keeping the touched location in focus, and the needle with the single particle or two is now reattached in its place. The particle is now brought into contact with the adhesive spot on the cantilever and the needle is

withdrawn. The cantilever is quickly removed and allowed to cure overnight in a secure AFM chip container with a gel pad.

One of the challenges addressed during the particle attachment process includes static attraction of the particle to syringe needle. Since the base of the syringe needle is made of an insulating material, a charge gradient may exist between the two tips resulting in immediate attraction of particles to an undesired location along the tip. This often occurs in dryer conditions. The way around this is to couple the two syringe needles using a conducting copper wire which will bring both tips to the same potential and thus eliminate undesired transfers of particles from needle tip to needle tip.

Drawn glass fibers were also utilized by heating and drawing glass rods instead of the syringe needles, however, inconsistencies with the particle deposition resulted since often times the drawn capillaries were difficult to image with the microscope. There were also issues with isolating particles due to static interactions which couldn’t be dissipated as easily as with a metallic needle tip.

Another challenge was finding an adhesive which would work well to adhere the particles and maintaining adhesion in various liquid media. Three types of epoxy resins were used and glass bonder super glue. The consistency of the adhesive served to be the primary concern. The less viscous super glue was difficult to handle due to its rather quick drying times. Utilizing smaller scale volumes of the fluid which cured even more rapidly made it nearly impossible to adhere a particle to the cantilever. A 60 minute epoxy-resin compound exhibited issues on the other end of the spectrum. Although the system allowed for a gradual increase of viscosity, which enhanced the ease by which the adhesive could be applied to the cantilever, the lengthy curing times meant that the

particle could shift positions along the cantilever and result in undesired final configurations. The most useful system was that of the Bisphenol A epoxy resin with a mercaptan terminated polymer hardener with a 5 minute cure time. The epoxy system exhibited low viscosity allowing it to be easily deposited onto the cantilever, but also increased in viscosity to a tacky medium by the time a particle is introduced. This ensured the particle remained fixed while the epoxy cures.

Other methods of adhering particles to the cantilever are present in the literature from the use of UV-curing optical adhesives to waxes which allow viscosity control with temperature. However, these were not examined due to lack of availability and requiring complicated setups. Furthermore, it was found that a more easily acquired epoxy served our purposes. Cured Loctite 5 minute epoxy resins were immersed into the tested solvents to determine whether any degradation issues could be found. In the time scale of the experiments, i.e. on the order of 1 hour, no discernible change in the epoxy was observed.

Finally, the cantilever type plays a major role in the adhesion of the particle. Initial usage of a triangular contact cantilever or a silicon tapping mode tip was chosen since its center point could easily be identified using the optical microscope (see Figure 4-4). Unfortunately, due to the limited attachment points, the particle adhesion could not be maintained in the presence of a fluid environment.

Tipless cantilevers were purchased from MikroMasch. The cantilevers are quite versatile since each chip contains 6 rectangular cantilevers of various spring constants. The rectangular cantilevers also facilitated the ability to determine the center axis by noting the angle required to focus from one edge to the other and then dividing that by

half. Furthermore, a larger volume of epoxy can be placed upon one of the cantilevers, and then using a clean syringe needle, a small amount of the adhesive could be acquired and rapidly transferred to a neighboring cantilever. See Figure 4-5 for the manufactured colloid probe utilizing the tipless cantilever.

Once the system is completely cured (~48 hours), the cantilevers are submerged in deionized water and rinsed with methanol multiple times to ensure adhesion. The colloid probes can be examined easily using an Olympus BX-60 optical microscope in reflection mode.

Summary

Modifications were made to the liquid cell of the Multimode AFM system to allow it to be compatible with a wide variety of organic liquids. Primarily, the lack of chemical compatibility of the silicone parts with ethers and other aggressive organic solvents required new materials selection. Thus, a Kalrez O-ring was modified to fit into the grooves of the quartz liquid cell, PTFE tubing was connected, and glass syringes were used to ensure complete compatibility with a diverse set of organic liquids.

Furthermore, the process and protocol of particle attachment has been provided to address various challenges, such as adhesion and electrostatic issues, which might present themselves during the manufacturing of colloid probes. Having the proper tools, the next step is to utilize them in measuring interactions.

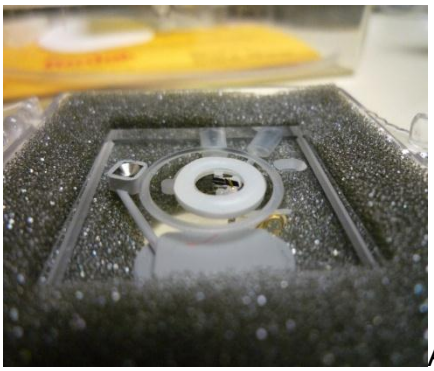
A

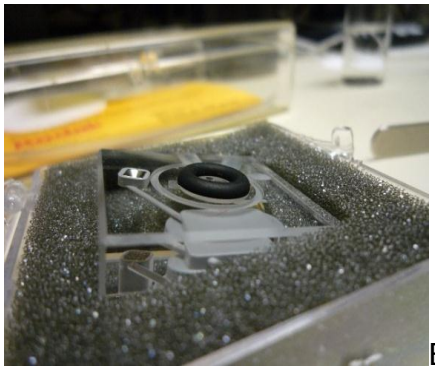
B

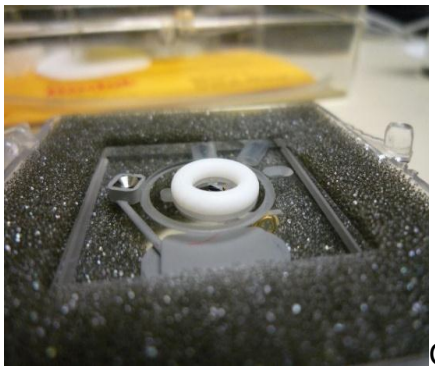
C

Figure 4-1. Various O-rings materials for Multimode AFM fluid cell. A) Silicone O-ring. B) Kalrez O-ring (unmodified). C) PTFE O-ring (unmodified)

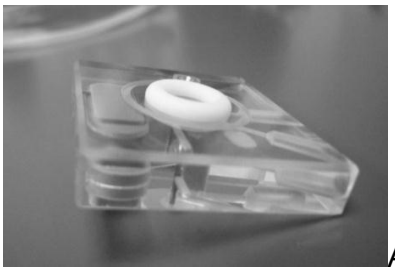
A

B
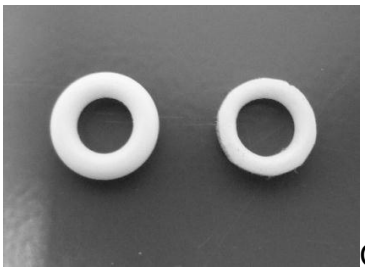
C

Figure 4-2. O-ring modification to fit into fluid cell groove. A) Original O-ring which does not fit well into groove. B) After modification of inner and outer diameter, the O-ring fits nicely. C) Modified O-ring compared with unmodified.

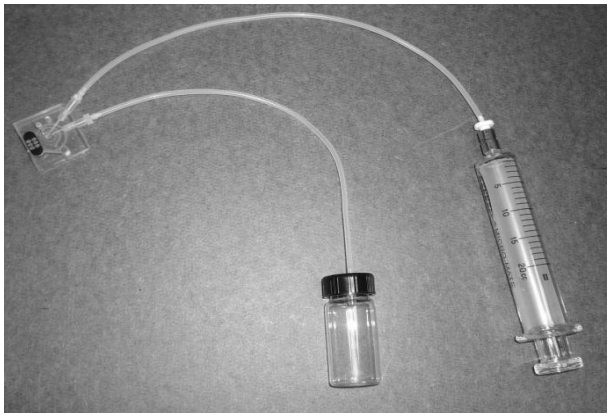

Figure 4-3. Liquid media containment system. Glass pipette is shown with PTFE fitting attached to PTFE tubing and connected to inlet port. The outlet port is connected to modified glass vial to prevent solvent evaporation into the environment.

Figure 4-4. Optical light microscopy of particle attached to an AFM contact mode silicon nitride cantilever with pyramidal tip. The particle is 7 µm in diameter.

A

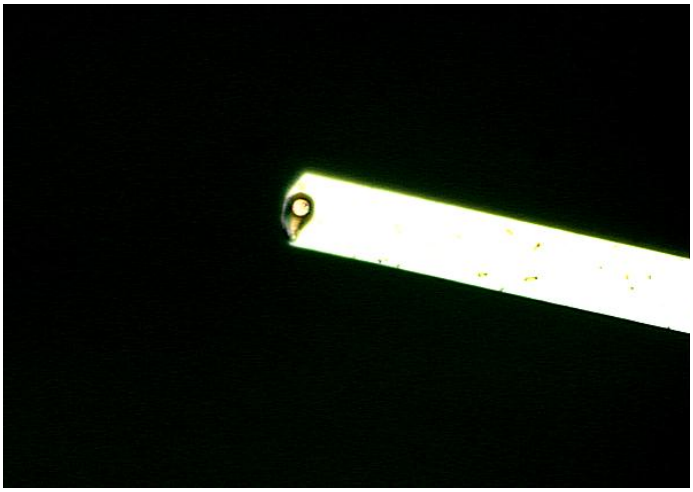

B

Figure 4-5. Optical microscopy of tipless cantilever. A) Tipless cantilever without particle seen from the side. B) Final colloid probe shown from the top down. Particle size is 7 µm.

CHAPTER 5
FORCE INTERACTION MEASUREMENTS

Overview

With the modifications to the liquid cell and the construction of colloid probes addressed, experiments can begin in the liquid media. The focus of this chapter is to establish experimental parameters and to effectively ensure consistent and reproducible force curves and conditions which don't damage the colloid probe. Furthermore, the goal is to determine whether real world phenomena correspond to the predicted interactions and whether the hypothesis that the vdW interaction force dominates the attractive interactions of the system is supported.

First, the experimental methodologies are detailed as to how to go about determining the contact area, the spring constant, and other parameters to facilitate force curve interaction measurements. Data manipulation, results and analysis finally are provided with regard to the liquid systems of interest in the context of colloidal forces.

Characterizing Contact Regions

Historically, when measuring interactions between a colloid probe and a corresponding flat surface, authors assume that the particle size is the size of the interaction. Unfortunately, this might not be the case for real world particles exhibiting surface topography such as open pores and asperities. At such small length scales, the geometry and local interacting region may not be what is macroscopically determined.

One of the more novel developments of atomic force microscopy is the implementation of reverse imaging allowing a probe or tip surface to be characterized and thereby being able to directly ascertain the effective interaction radius.[77] The

concept implements a grid with an array of uniformly sharp tips. The probe having a significantly larger radius of curvature than any of the tips is engaged to the grid and allowed to scan the surface. As the probe rasters along the stationary sharp tips, it feels a corresponding force from its surface topography which translates to imaging of the surface of the probe. The variations in height information can subsequently be used to calculate the actual particle radius interacting with a sample. Based on geometry and assuming a perfectly spherical particle, the corresponding radius of a particle can be determined by the following relationship:

$$R = \frac{h^2 + \left(\frac{w}{2}\right)^2}{2h} \tag{5-1}$$

where R is the interaction radius, h is the center height measured during imaging, and w is the width of the particle.

The TGT1 calibration reverse imaging grating was purchased from NT-MDT. Engaging a colloid probe and scanning the grating yielded an image with an array of circular regions representative of the particle surface (see Figure 5-1). The contact radius average and standard deviation were determined from six measurements, and was found to be 2.3 ±0.20 µm for the main silica probe used in the majority of non-aqueous experiments.

Determining Cantilever Spring Constants

As mentioned in the previous section, two atomic force microscopes were used. The Dimension 3100 was used to measure the cantilever thermal response and thus provide a quantifiable spring constant. Briefly, the thermal tuning process developed by Hutter et al. operates by measuring the cantilever's response to thermal energy in the

environment with time.[78] The result is then converted to a frequency spectrum of the cantilever's response corresponding to the power spectral density. Fitting the frequency spectrum to a Lorentzian shape and taking its area yields the power of the cantilever fluctuations which is then used to calculate the spring constant. The Veeco Nanoscope 5 software performs these calculations and further corrects for cantilever geometry and accounts for various other conditions of reality.[79]

Before the thermal tune method can be utilized, the deflection sensitivity of the cantilever needs to be determined to allow the deflection in volts to be converted to nanometers. The sensitivity is determined by contacting the tip to a hard surface and into a region of linear constant compliance, i.e. the voltage measured is proportional to the distance the probe travels. The reciprocal of the proportionality constant is termed the sensitivity and is usually given in nanometers per volt. The sensitivity needs to be determined again each time the cantilever is mounted.

By the thermal tune method, the main colloid probe used in most of the characterizations had a spring constant of 0.0720 N m^{-1} corresponding well with the company literature for an unmodified cantilever to exhibit a spring constant of 0.01 to 0.08 N m^{-1} with an average of 0.03 N m^{-1}. Theoretically, a rectangular shaped cantilever would have a spring constant, k, of:[80]

$$k = \frac{Ewt^3}{4L^3} \tag{5-2}$$

where E is Young's modulus, w is the width, t is the thickness, and L is the length. The effect of introducing the particle increases the effective thickness and thus increases the spring constant. Colloid probes were made having various spring constants measuring from 0.0328 N m^{-1} to 0.1495 N m^{-1}. This range is attributed to the

placement and amount of epoxy deposited onto the cantilever resulting in changes in the cantilever's effective thickness. Other techniques exist to determine the spring constant and can be categorized as theoretical determination from cantilever geometry and materials properties,[81-84] static measurements involving deflecting the cantilever with a known force,[85-87] and dynamic methods which determine the change in resonance properties.[78,88,89] The thermal tuning method belongs in the latter category and was used as it was the most convenient method and yielded consistent responses corresponding well within the manufacturer's specifications.

Liquid and Chemical Information

Deionized water was acquired from an in-house system (Barnstead EPure D4641), while ethanol (Acros Organics, 200 proof, ACS), 2-propanol (Fisher, certified ACS), methanol (Fisher, certified ACS), and THF (Acros Organics, 99.5%, stabilized) were purchased and used as received.

Atomic Force Microscopy Parameters

The Nanoscope 3-controlled Multimode AFM with the J-scanner and a fluid cell module was used to measure the force interactions between the probe and stainless steel surface. With the liquid cell set up with the cantilever and chemical compatible O-ring and brought close to the steel surface, a liquid medium needs to be drawn in to the cell before the laser is to be aligned onto the cantilever. It is suggested that the fluid be drawn into the fluid cell rather than pushed into it. The difference being that having a vacuum draws out the air bubbles which are inclined to travel towards a low pressure region rather than pushing an air bubble out which may be difficult and actually lead to breakage of the cantilever. Alignment could occur before drawing in the fluid to bring the laser near the desired tip location, but the fluid will change the refractive index of the

system and require realignment of the laser to the photodetector. Once fluid is drawn into the liquid cell and alignment performed, measurements can begin.

First, the system was set up to engage the surface in contact mode. A small 5 nm scan size is chosen with a very low engagement deflection voltage to ensure the probe isn't damaged when engaged. Then, the sensitivity had to be measured by activating the force-curve measurement mode. Identifying the sensitivity parameter allows for establishing the maximum deflection the cantilever should undergo during a force curve measurement and thus preserves the integrity of the tip and cantilever during subsequent tests.

The spring constant measured earlier allows for the nm deflection to be converted to Newton force units. Force curves of at least four different locations (usually 5 locations) separated by 5 µm were acquired using a 10 nm or 20 nm trigger feedback mechanism to limit mechanical deformation of the particle probe. These values correspond to forces of 0.72 nN or 1.44 nN. In order to exceed the compressive strength of silica (1.1 GPa), the interaction would have to occur on a circular area with a radius of less than 0.65 nm. Furthermore, the tensile strength of silica is 50 MPa, so in order to exceed this value, the circular interaction radius must be less than 3 nm. The silica sphere porosity is also a factor to decreasing its strength and increasing the minimum radius of interaction required before mechanical failure.

The characterization was set to obtain deflection measurements at a range of 50 – 200 nm and incrementing at 1 nm with a scan rate of 1 Hz, corresponding to a tip velocity of 100 nm s^{-1}. Once the tip reaches a contact deflection corresponding to 10 or

20 nm, the scan stops incrementing and continues to retract and engage upon the sample acquiring force curves over time.

Force Curve Results

Force Curves in Non-Aqueous Liquid Conditions

Representative force curves in methanol for the silica are shown in Figure 5-2. Note there are two curves which indicate the measurement as the two surfaces are brought into contact, termed extended (Ext), and when the surfaces are separated, termed retracted (Ret). The acquired voltage-displacement curves were converted to force-displacement by multiplying the voltage by the sensitivity to obtain a deflection-displacement curve, and then using the spring constant to convert the deflection to force-displacement information. To convert displacement of the cantilever to a separation distance or the distance away from the particle surface, a point of contact had to be determined. This point of contact was established by using the Nanoscope software to determine deviation from the linear constant compliance region and establish that as the point of contact, at times manual adjustments had to be used to shift the curve along the x-axis. Finally, the forces were normalized by dividing by the particle interaction radius determined earlier using the TGT1 reverse imaging grid.

Various properties can be extracted from the force-curves. From the extended curves, the attraction distance can be determined from the distance away from contact as well as the magnitude of the attraction based upon the snap to contact depth. From the retract curves, the adhesion can be measured by the depth of the curve before the silica probe is pulled off from the steel surface. Focus, though, is placed on the extend curve and the forces experienced by a particle as it approaches the steel surface since these were the most reproducible.

Figure 5-3 shows the force curve profiles at 5 different locations on the steel surface. The values correspond to a starting point defined at (0,0) and then measuring (+5 μm,0), (-5 μm,0), (0,-5 μm), (0,+5 μm) and back again at (0,0). The curves have been offset slightly to show that overall, the jump to distance remains relatively constant and without much deviation, and furthermore, the magnitude of the attraction is reproducible. What appears to be long range repulsion beyond 30 nm stems from laser interference effects which often occur when examining reflective surfaces[90-92] such as the steel used in these experiments, rather than from the effects of silica gel or hairy layers which often lead to short-ranged non-DLVO repulsion.[11,93] These optical interference effects present themselves as periodic wave-like signals. There might also be slight contributions from pressure differentials formed in the cell while the piezo compresses the volume of the cell environment in order to bring the cantilever to engagement upon the surface.

Taking the average and standard deviation from the five measurements for the interactions in the methanol liquid environment, the silica particle was found to experience attractive forces of 0.17 ± 0.04 mN m^{-1} at a distance of 11 ± 1.4 nm (Figure portrays mean and standard errors while values reported in the text are standard deviation).

A representative force curve for THF is shown in Figure 5-4. Note that the hump is an artifact caused by the laser interference as was present in the methanol force curves. Interestingly, upon retract, the contact region interactions are slightly different as represented by the separation of the retract from the extension curve. This hysteresis

effect might be the result of fluid dynamics,[94] but doesn't appear to exhibit the long-range adhesion typical of a meniscus effect.[95]

The THF system exhibits over a magnitude of diminished attractive and adhesive forces between the silica and steel surfaces compared to the methanol system. The force of attraction goes from nearly 0.2 mN m^{-1} and adhesion of 0.4 mN m^{-1} in methanol to corresponding extend and retract profiles indicating no attraction and less than 0.01 mN m^{-1} adhesion in the THF system. The use of THF would provide a lubricating wall surface during processing where silica particles may be forced along the surface of the steel without the need for long-chain organics. Furthermore, in such applications such as column packing, rinsing with methanol should provide enhanced attraction and adhesion to the wall surfaces and might facilitate maintaining the internal pressure which could improve column stability.[96]

Comparison with the theoretical model developed in Chapter 2 and 3 facilitates the interpretation for the processes and mechanisms that occurred to achieve the measured results. The model provides calculated Hamaker coefficients whose values can be inserted into the vdW force equation. Dividing both sides by the radius of the particle, the equation now represents the normalized force interactions which can be directly compared to experimental results.

As the separation distance, d, decreases the vdW interaction becomes more and more significant. The relationship is in good accord with the interaction of the silica surface against steel in methanol. Solving the vdW equation for when the particle is expected to experience a force/radius equal to 0.17 ± 0.04 mN m^{-1}, we find a distance of 8.0 – 10.2 nm. This range compares to the measured 11 ± 1.4 nm obtained from the

experiments, and thus verifies that the attractive force measured is derived predominantly from the effects of vdW interaction between sphere and steel surfaces.

For the silica sphere in THF, good agreement with vdW calculation was determined. From the calculated Hamaker coefficient determined, the vdW repulsive force should increase with decreasing separation. A comparison of the vdW calculated values with the experimental data is shown in Figure 5-5. In fact, other than the optical interference region, there appears to be very good agreement between experimental and theoretical calculations at the short distances where vdW interactions are expected to be dominant and measureable. Thus, vdW repulsive interactions were achieved.

During retraction, the residual adhesion of 0.02 mN m^{-1} upon pull off indicates there to be a slight attractive/adhesive interaction. The contact mechanics caused by mechanical deformation during approach result in residual adhesive interactions.[97,98] Furthermore, the adhesive force might result from trace surface water molecules leading to an attractive capillary forces at short distances.[5]

Further solvents testing in the presence of ethanol and 2-propanol against steel was completed, and the force interaction results are presented in Figure 5-6 and with the attraction-distance presented in Figure 5-7. Of the four solvents tested, ethanol exhibited the longest jump in distance of 20 nm with a force interaction at 0.1 mN m^{-1}. 2-propanol also exhibited weak short-range attractive interactions on the order of 0.05 mN m^{-1} at 2.5 nm. This is much less than the interaction predicted by calculations where vdW attractive interactions should have become significant at 0.1 mN m^{-1} by a 10 nm separation distance. The lack of vdW attraction based upon the theoretical calculations suggests the presence of long-range repulsive counteracting interactions between silica

and steel in these solvents. An explanation for this is the presence of trace water in the solvents which might form strong hydrogen bonds with the surface groups of silica and result in short-range repulsive hydration forces on the order of 3-5 nm, with the roughness of the particles smearing out the normally oscillatory force into a monotonic hydration repulsion.[99,100]

Force Curves in Aqueous Conditions

Force curves in aqueous conditions were completed using the AFM 3100 with a Dimension V controller and liquid cell due to convenience. Water is able to easily bead up on the stainless steel surfaces and there aren't any concerns with the chemical compatibility of salt water with the silicone skirt used to shield the liquid cell from the electronics. To use this set up, the tip is brought close to the steel surface, and then a plastic transfer pipette is used to deposit a bead of water between the two surfaces resulting in a water column. Again, the laser is aligned and steps are carried out to determine the probe's sensitivity and spring constant. The spring constant for this probe was measured to be 0.0328 N m^{-1} and the tip interaction radius was 2.93 µm.

The extended curve results are shown in Figure 5-8. The maximum attractive force during jump-in goes from 0.37 to 0.19 and finally to 0.07 mN m^{-1} when increasing the monovalent salt concentration from 10^{-3} M to 10^{-2} and 10^{-1} M, respectively. Also, from the figure, the jump-in distance goes from 40 nm to 25 nm to 10 nm for low, medium, and high concentrations of salt, respectively. At the high salt concentration, the system is dominated by van der Waals interactions due to screening of the EDL. Calculating the Debye length, which gauges the thickness of the double layer, for each of the salt concentrations, we obtain 9.6, 3.0, and 0.96 nm for the respective low, medium, and high concentrations of salt.

The Hamaker coefficient was calculated for the silica-water-Cr_2O_3 and silica-water-silica interactions using the MathCAD spreadsheet and was found to have a value of 3.48 x 10^{-20} J and 7.22 x 10^{-21} J, respectively. The silica-water-silica Hamaker coefficient corresponds well with values found in the literature.[101] Placing the Hamaker coefficient value for silica-water-Cr_2O_3 into the force interaction equation, we find that at 10 nm, which corresponds to the approximate jump-in distance of the screened EDL conditions, the vdW force is expected to be on the order of 0.06 mN m^{-1}. This value is less than that of the attraction force of 0.07 mN m^{-1} measured at high salt concentrations.

The excess attractive interaction is believed to result from a combination of EDL and vdW effects. The aqueous environment exhibited a neutral or slightly acidic pH (due to adsorption of carbon dioxide present in the atmosphere). The isoelectric point of silica occurs around a pH of 1-3.[102] This means that silica would have a net negative charge under the experimental conditions. From the literature, chromium oxide has an isoelectric point at a pH of 9.2,[103] giving it a positive surface charge under slightly acidic to neutral conditions. This should yield purely attractive interactions between the two surfaces. Parametric analysis was conducted using the DLVO model assuming that the silica exhibited a negative Stern potential of -75 mV, with monovalent electrolytes, a Hamaker coefficient of 3.48 x 10^{-20} J, at room temperature, particle radius of 2.93 µm, and assuming constant potential. The Stern potential of the steel surface was altered until the electrolyte concentrations' large dominant vdW attractive interaction force could match up similarly with where the experimental data exhibited its attractive jump-in

forces. This occurred roughly at a steel surface Stern potential of 95 mV, see Figure 5-9.

Initially, when plotting the force curves on a log-plot, the repulsive regions just before jump-in for the 10^{-3} M and 10^{-2} M salt concentration were found to exhibit linear trends which corresponded well with theory about the exponential decay of the EDL force. The electric double layer repulsion was actually unexpected due to the difference in surface charges of the silica and the steel in the aqueous environment. Still, attempts were made to use DLVO theory to try to match up the force interaction curves of the experiment, by assuming that both surfaces exhibited negative Stern potentials. However, unreasonable values were obtained, i.e. extremely large potentials on the order of -700 mV on one surface compared to -7 mV on the other and requiring changing the Hamaker coefficient to values on the order of 1×10^{-21} J to yield similar force profile curves at the low and medium salt conditions. Thus, there must be some other non-DLVO contribution which exhibits an exponential decay at long range distance.

Initially, it was thought that the repulsion was due to the effects of long-range hydration forces which also exhibit an exponential decay. However, this force is expected to operate on the order of 3-5 nm.[5,99,100] Parsegian and Gingell demonstrate that there are EDL conditions where oppositely charged surfaces with of different magnitudes can exhibit repulsive interactions depending on their surface charge ratio and separation distance when ions in solution are restricted into the region between the surfaces.[104] However under these conditions, the EDL forces should remain repulsive

and not lead to the slight increased attraction observed during testing with decreasing salt concentration.

Furthermore, it becomes easy to see why polymeric dispersants are used to maintain colloidal stability in an aqueous system. There are often times when multiple components exhibiting differing surface charges interact hindering or compromising colloid stability. Using organic liquids with high vapor pressures has the potential to address these issues and would allow for ease in recovery rather than requiring burning off of the organics later on during processing.

Settling Study of Particles in Various Liquids

With any selection of solvent to alter interactions between particle and wall, the effect on particle-particle interactions is also important to consider. Settling studies were conducted for the silica particles using the solvents mentioned in the previous section. Clear 5 mL glass vials containing 0.25 g of silica powder were filled with 2.5 mL of solvent. The vials were ultrasonicated for 5 minutes to break apart any agglomerates and then hand-shaken before analysis of the sedimentation. Analysis was completed by taking still frame images at various intervals and plotting the height of the particle-supernatant boundary (see Figure 5-10). For systems which quickly settled, video was used. Images and videos were processed to enhance contrast so as to facilitate and standardize the identification of the moving boundary. The height of the moving boundary was measured by drawing a line to the corresponding height on a ruler situated next to the vial. The slope of the initial linear region was used to determine the measured settling rate.

The results are presented in Figure 5-11 and show that 2-propanol exhibited the most resistance to settling by the silica system whereas THF actually encouraged rapid

sedimentation. Silica in methanol also settles rapidly compared to the other solvents tested.

Comparing with theoretical calculations on settling, the velocity of a particle settling in a gravity field was determined by using the Stokes equation:[21]

$$v_s = \frac{2}{9}\left(\frac{\rho_p - \rho_f}{\eta}\right) g R^2 \tag{5-3}$$

where v_s is the Stokes velocity, ρ_p is the density of the particle, ρ_f is the density of the fluid, η is the fluid viscosity, g is the gravitational constant, and R is the radius of the particle. Viscosity and density values for the solvents were obtained from the literature.[105] In the calculations, the particle has a radius of 3.5 μm and density of 2.2 g cm^{-3} as found in the literature.[106] The settling behavior is in agreement with Stokes law trends, see Table 5-1, but exhibits decreased velocities compared to the calculations.

Accounting for porosity requires a modified version of the Stokes equation:[107]

$$v_s^* = \left(\frac{d^2\left\{\rho_p\left(1 - \in_i\right) + \rho_f\left(\in_f - 1\right)\right\} g}{18\eta}\right) \tag{5-4}$$

where d is the particle diameter, ϵ_f is the fraction of pores filled with fluid assumed to be 0.3, and ϵ_i is the porosity of the particle represented by:

$$\in_i = \frac{V_{pore}}{V_{pore} + \frac{1}{\rho_p}} \tag{5-5}$$

where V_{pore} is the volume of pores. For Zorbax SIL, this value was found in the literature to be 400 μL per gram.[108] The porosity-modified Stokes velocities were calculated to be 2.79 x 10^{-2}, 2.85 x 10^{-2}, 1.59 x 10^{-2}, and 8.59 x 10^{-3} mm s^{-1} for THF, methanol, ethanol, and 2-propanol, respectively, neglecting undetermined particle-

solvent-dependent constants and the effect of solids loading. Comparison to measured values show that the measured particle velocity in THF is 0.95 of the calculated value and about 0.5 for the other solvents tested. Furthermore, the effect of porosity suggests that the particles in methanol should settle the fastest. This was not observed but the increased settling by THF might be attributed to vdW attraction-induced agglommeration. The other contributions decreasing the rate of settling are believed to come from solids-loading effects[107] and solvation forces from confined solvents between particles[5] which lead to repulsive interactions.

The calculations for Hamaker coefficients for a silica sphere interacting with a silica sphere in these solvents yield the following values: 5.481×10^{-20} J for THF, 2.337×10^{-20} J for methanol, and 1.938×10^{-20} J for 2-propanol. Larger values of the coefficients correspond to a greater magnitude of vdW attractive forces and thus, sedimentation rates are expected to be greatest for THF, then methanol, and finally 2-propanol having the lowest rate assuming only vdW attractive interactions. This trend is similar to the Stokes velocity calculations with the THF environment causing silica to settle much more rapidly than in methanol and furthermore, with 2-propanol exhibiting the lowest agglomeration and settling rates for the silica spheres. Effectively, the settling rates observed are due to gravitational effects as well as other interparticle interactions which counter the settling such as solvation and solids loading effects.

Summary

Force curve measurements determined that under non-aqueous environments, methanol led to silica-steel interactions which are in close agreement to the predictions determined by vdW force calculations. Furthermore, the THF solvent led to the complete reduction of attractive force interactions between the two surfaces and

exhibited a profile corresponding to the vdW repulsive interaction force calculations. However, THF might not be the most desired solvent to use in real world systems since though it may provide lubrication to silica particles encountering steel walls, the liquid media might actually agglomerate the particle system and result in difficulties to efficiently transport the particles. Furthermore, THF poses significant health and toxicity hazards and forms explosive peroxides when not stabilized with preservatives such as butylated hydroxytoluene; thus its use here is meant to be as model. Based on the results of this section and the previous, it would appear that 2-propanol would be the most effective solvent in transporting silica spheres through stainless steel tubing. The Stokes interaction indicates that the particles would settle and agglomerate slowly in the solvent, and the measurements of particle-wall interactions furthermore indicates low attractive interactions at short distances compared to the other alcohols.

Table 5-1. Stokes' law calculations compared with measured boundary velocity of particle-solvent system.

Solvent	Fluid density ($g\ cm^{-3}$)	Viscosity (cP)	Stokes velocity ($mm\ s^{-1}$)	Measured velocity ($mm\ s^{-1}$)
Tetrahydrofuran	0.888	0.55	6.37E-02	2.65E-02
Methanol	0.792	0.6	6.26E-02	1.62E-02
Ethanol	0.789	1.08	3.49E-02	8.80E-03
2-Propanol	0.786	2	1.89E-02	4.70E-03

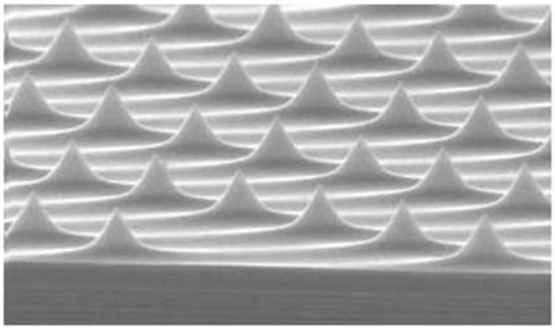

A

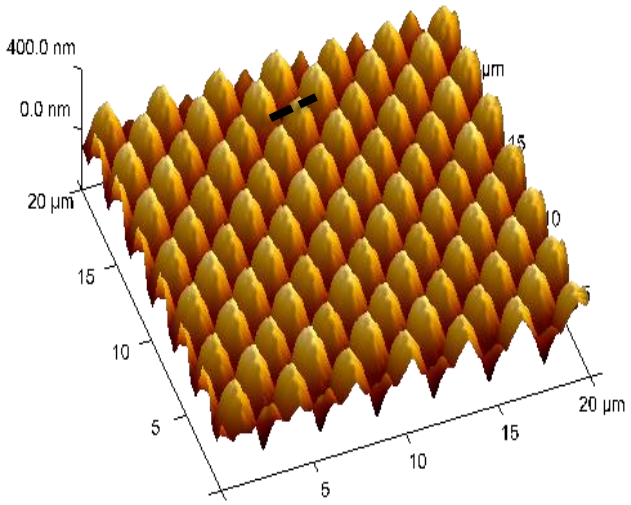

B

Figure 5-1. TGT1 reverse imaging grid and imaging of silica colloid probe. A) Reverse imaging grid topography. B) Three-dimensional array representation of multiple images of scanning colloid probe resulting from scanning probe along reverse imaging grid.

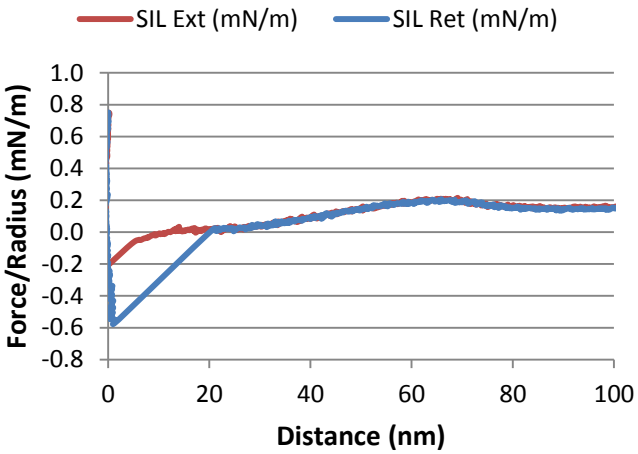

Figure 5-2. Representative force curves of silica against stainless steel in methanol.

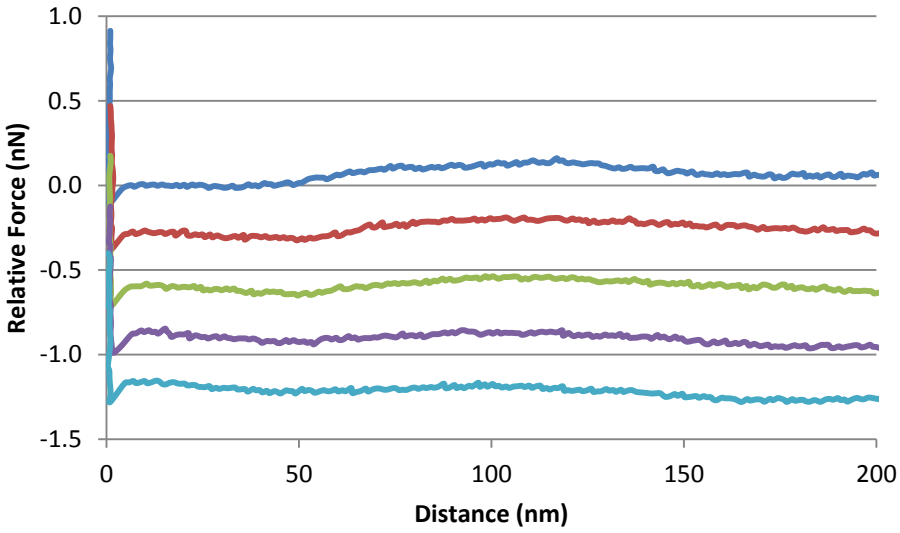

Figure 5-3. Reproducibility of force curve. Force curves of silica extended towards steel in methanol showing consistency of data acquired.

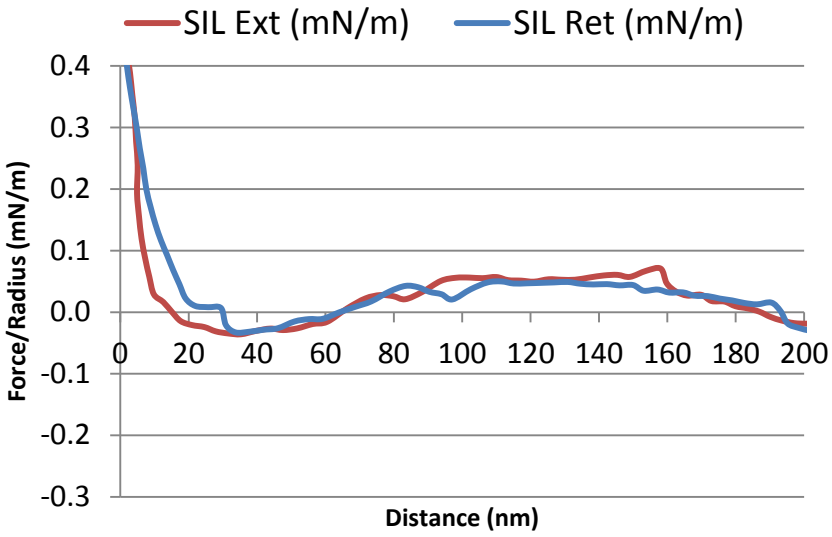

Figure 5-4. Representative force curves of silica against stainless steel in THF.

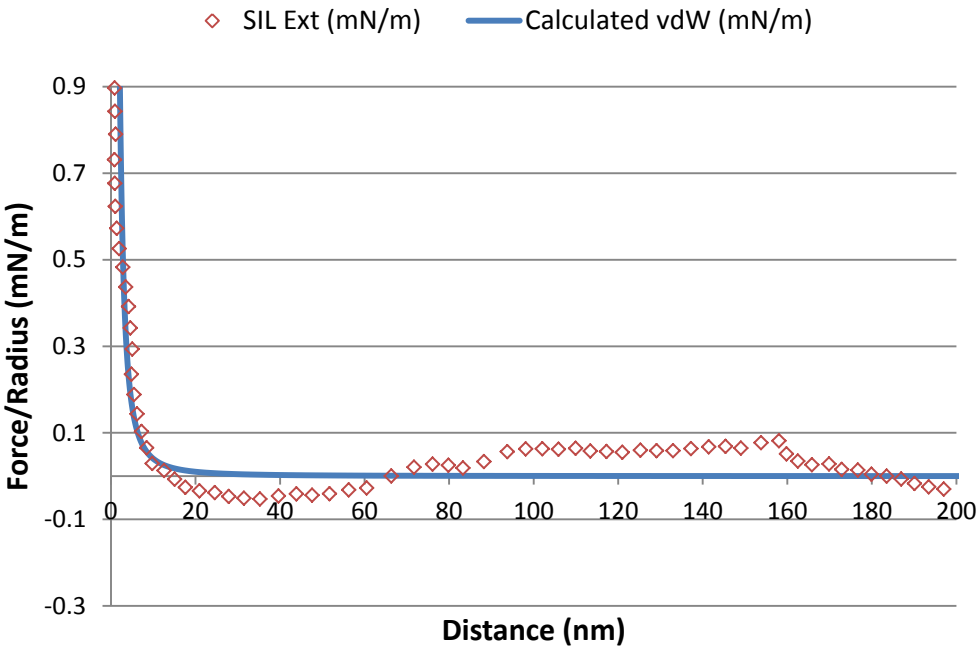

Figure 5-5. Comparing force interactions in THF with theory. The vdW calculation was determined using the calculated Hamaker coefficient of -2.41 x 10^{-20} J. Good agreement between experimental and theoretical calculations indicates vdW repulsive interactions were achieved for silica interacting with steel in the presence of THF.

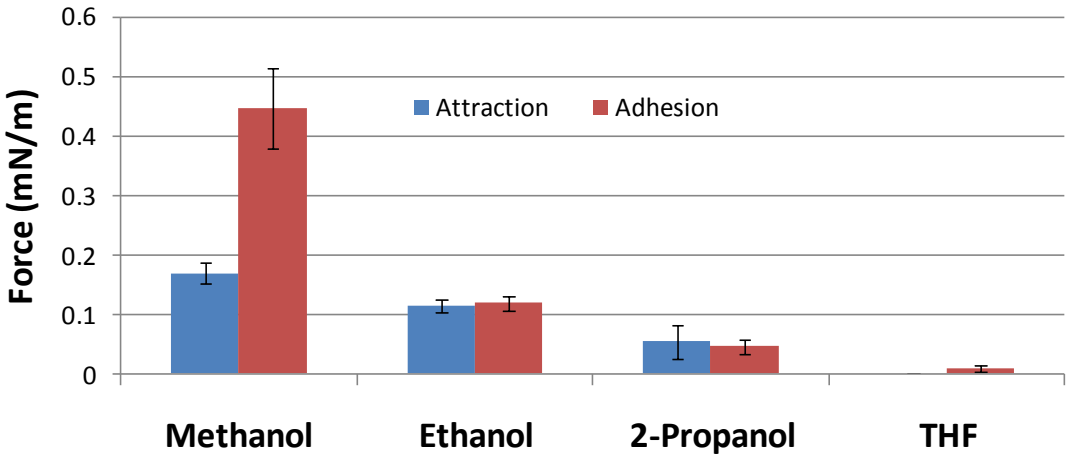

Figure 5-6. Attraction and adhesion strength of silica against stainless steel in various liquid media.

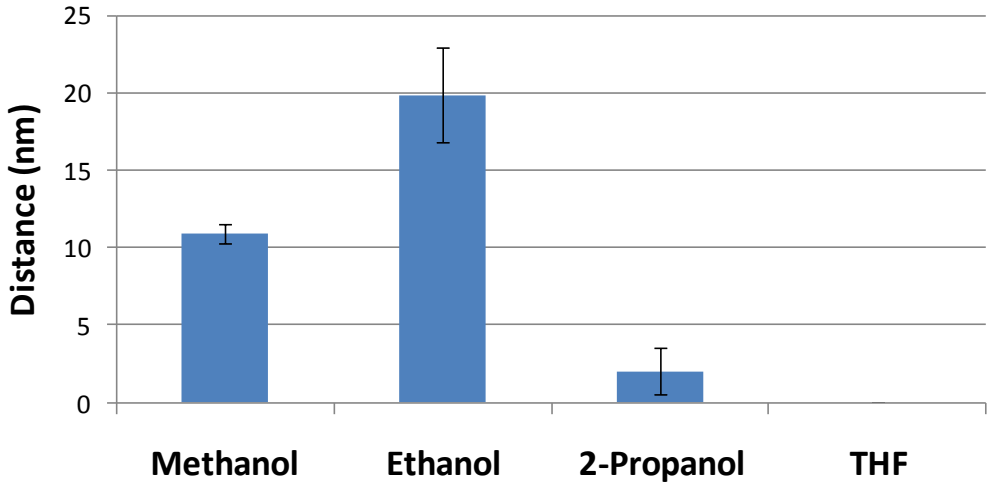

Figure 5-7. Distance of jump-in measured for attraction of silica against stainless steel in various liquid media.

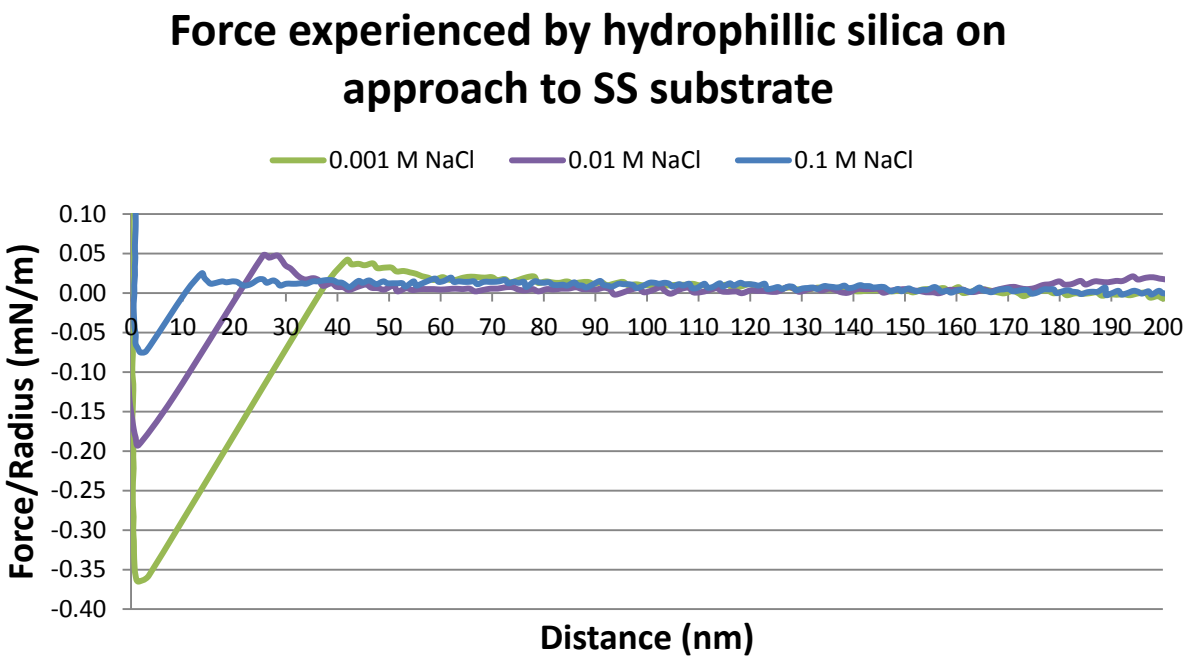

Figure 5-8. Force interaction curves of silica against stainless steel in the presence of aqueous liquid media containing various concentrations of salt.

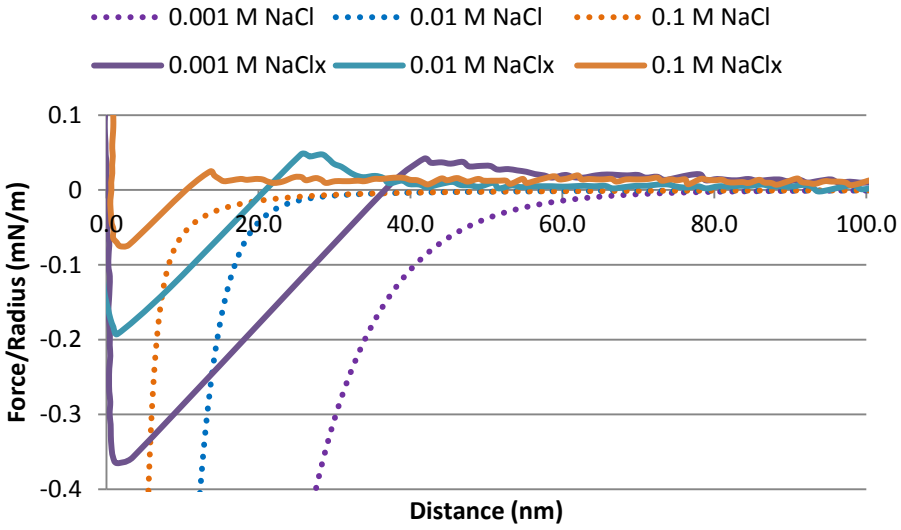

Figure 5-9. Comparison of DLVO calculation with experimental results. The solid lines represent experimental values and the dotted lines represent the calculations assuming a silica Stern potential of -75 mV and a steel potential of 95 mV.

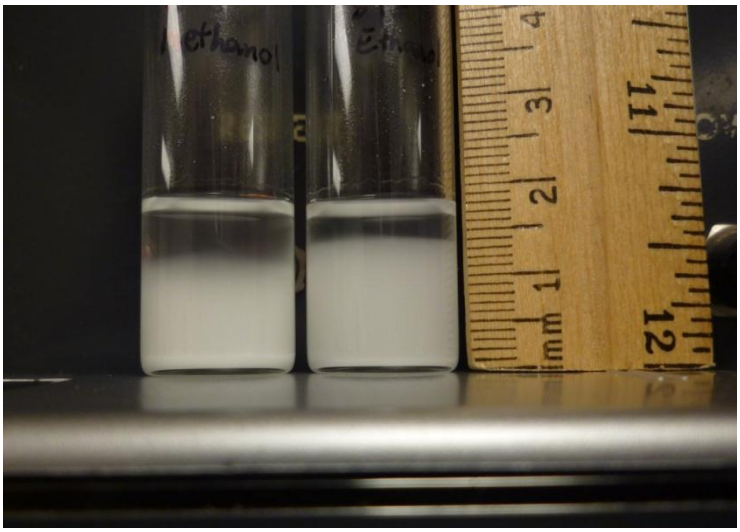

Figure 5-10. Settling experimental setup. Glass vials containing particles are ultrasonicated and hand-shaken and allowed to settle. The ruler is used as a guide to measure height over time.

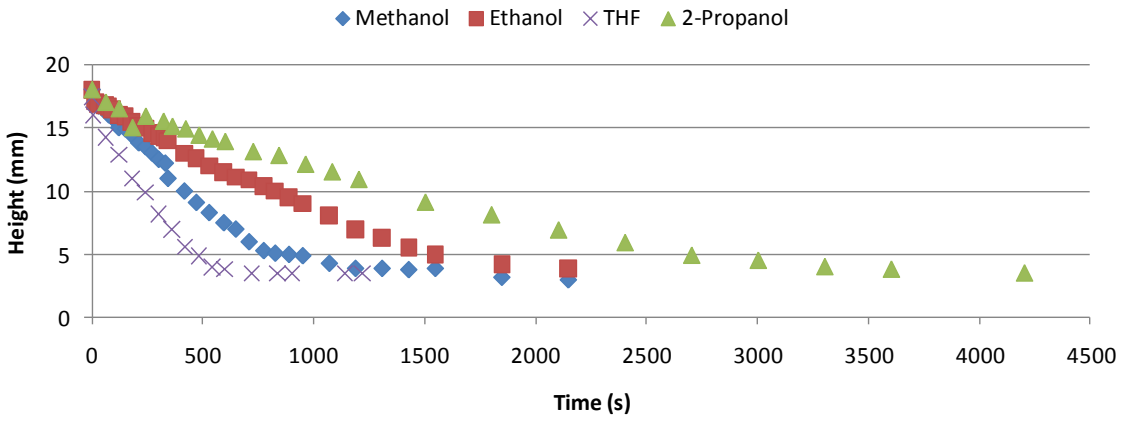

Figure 5-11. Settling profile of silica in the presence of various solvents.

CHAPTER 6
CONCLUSIONS AND FUTURE WORK

Conclusions

Towards producing a completely polymeric dispersant-free processing medium for ceramics, the silica sphere system was introduced and its interaction with stainless steel under various liquid solvent media conditions were characterized and evaluated. This process required addressing the challenges of instrumentation and solvent compatibility as well as developing a suitable colloid probe. To make the AFM fluid cell less susceptible to chemical attack by the various solvents of consideration, Kalrez O-rings were used to substitute for the original silicone fitting. Furthermore, PTFE tubing was incorporated as well as glass syringes. Colloid probes constructed using tipless cantilevers were produced utilizing an epoxy which exhibited good chemical stability and solvent resistance.

Predictions were developed from the science of fundamental force interaction of colloids, and pure solvents were selected to represent a variety of interactions between the model silica sphere and a stainless steel wall. These systems were then tested and analyzed providing quantification of the interactions of the two surfaces. The results show that though THF effectively minimizes the attractive interactions and even reversing the normally attractive vdW interactions between silica and steel, concerns about its suitability lingers due to the lack of colloidal stability in the medium. Furthermore, despite using porous particles, in the presence of methanol and THF, the silica behaved in good accord with theoretical force calculations for purely vdW dominated system. The most effective solvent examined to mitigate attractive interactions between both particles as well as walls was found to be 2-propanol which

exhibited a 70% less attractive interaction force than methanol and a very small jump-in distance of 2 nm compared with methanol's nearly 11 nm.

Facilitating the use of pure solvents-based processing techniques requires some more work to be done. Though the fundamentals of predicting interactions and a system and protocols to characterize these interactions have been established, further quantification of the particle-particle interactions in various solvent media needs to be addressed. This is the subject for the future work section which consists first of designing mixed solvent systems to tailor the optical properties and dielectric response function of the liquid media. Then, a detailed discussion on how to characterize particle-particle interactions using a surrogate surface is provided. Through these developments, science-based solvent selection and efficient and more environmentally effective processing of ceramic particles can be brought to maturity.

Future Work

Refractive Index Matching of Liquids

One of the proposed notions of tailoring the particle-particle interaction is through the use of mixed solvents systems. Fluid mixtures allow the refractive index to be controlled directly, which impacts the vdW interaction. A liquid exhibiting a similar dielectric response behavior as silica would minimize the attractive vdW interaction. Furthermore, since refractive indices form a core component to the determination of the response, liquids with similar refractive indices to silica would result in decreased attraction between particles and may result in colloidal stabilization without the need for polymeric dispersants.

Silica exhibits a refractive index of approximately 1.40-1.50, thus, mixtures of liquids to yield this value is desired to minimize attractive interactions. A lot of common

liquid solvents exist with lower refractive indices such as methanol, with a refractive index of 1.33. However, to have a refractive index of greater than 1.4 means using rather hazardous solvents which can be found in various handbooks and databases.[105,109]

A quick study to determine how refractive index changes in mixtures of THF, chloroform, and p-xylene with methanol was undertaken. Mixtures by weight percent were made in 20% increments from pure methanol to pure high refractive index solvent. The refractive index was then measured using a Fisher brand Abbé refractometer calibrated to a naphthalene bromide standard.

Abbé refractometer

Briefly, the refractometer consists of two prisms forming a narrow space where a layer of fluid is deposited. Diffuse monochromatic 589.3 nm wavelength sodium light enters one prism, interacts with the solvent and refracts into the other prism according to Snell's law. The resulting light then enters a telescope. Next, the telescope is effectively moved until a sharp division of bright and dark regions occur at cross wires seen in the scope. This represents the critical angle and the point corresponds to a particular refractive index which is read off a calibrated scale.[110]

Results of refractive index measurements of liquid mixtures

The refractive index results were plotted against weight fraction, mole fraction, and volume fraction to determine which exhibits the best linear fit. Methanol exhibited a refractive index of 1.327, THF had 1.406 (which is actually less than the refractive index of the silica particles since the particles could still be observed when settling studies were conducted in THF), chloroform has 1.444, and p-xylene had 1.494. The most linear responses were found to be for the refractive index vs volume fraction plots.

Results with linear trend relationships are shown in Figures 6-1, 6-2, and 6-3. In order to design a solvent system having a similar refractive index as silica particle, mixtures of methanol with volume fractions of 0.930 THF, 0.640 chloroform, or 0.44 p-xylene could be made and the effects on surface force interactions tested between the silica particles.

Towards Characterization of Particle-Particle Interactions

Characterization of particle-particle interactions has often been accomplished on a macroscopic scale. Settling studies can provide some relative indications of how particles interact to form heavy agglomerates and the density of the resulting packed sediment can be used to relate to the adhesion experienced by particles upon contact. However, one of the fundamental limitations of this measurement technique is that particles in liquids having a similar refractive index are nearly impossible to visually observe. As mentioned before, since the refractive index can often be used to estimate a material's dielectric response function, as a first approximation, refractive index-matched liquids to a particle system may minimize the attractive interactions by particles. The challenge is to quantify the surface interactions between particles which are optically invisible.

One way of going about this is through rheological and viscosity measurements which can determine the relative conditions of flocculation during a dynamic, flowing system. However, such a process often requires a great deal of samples both particles and liquid medium and may be cost prohibitive. In order to obtain quantitative results, the most effective instrument to use is the AFM but this poses more challenges.

Attempts were made to directly measure the particle-particle interactions using a colloid probe. First, a thin layer of epoxy was placed onto an AFM specimen disc. Then,

a razor blade was used to quickly deposit a thin layer of particles onto the epoxy. Once cured, the disc was examined using the Dimension 3100 AFM using a silicon tapping tip, see Figure 6-4. Immediately, the challenges of force curves measurements are apparent. First of all, the particles are not evenly distributed on the surface and it would be challenging to obtain reproducible results since interaction can be with particle or with epoxy regions. Furthermore, the surface would have to be scanned first to determine where particles are located, and then the tip swapped out for the colloid probe to perform force curve measurements.

A more effective way of determining particle-particle interactions would be to utilize a flat surface which exhibits similar chemical properties as the surface of a silica particle. A silicon wafer would be a good example of a material to use since its surface chemistry can by modified by growing oxide layers through a simple and well-controlled thermal oxidation technique.[111] This occurs by heating a silicon wafer to 800- 1200°C and supplying a feed gas of either water vapor or oxygen. Water interacts with the silicon to form silicon dioxide and hydrogen gas, and oxygen interacts with the silicon directly to form silicon dioxide. Removal from the furnace would lead to the formation of silanol species on the surface and provide a very good analogue to the silica spheres. Thus, silica particle-particle interactions can be measured in various liquids using the protocols established in the previous sections.

Further studies could also address and characterize the internal and external interactions of hydrophobic particles through the use of the colloid probe. This would also be very desirable in the field of chromatography where silica particles modified with chains of carbon are used to form so called reverse phase columns. Conveniently, the

silicon wafer surface can be modified in the same manner that silica spheres are made hydrophobic, i.e. through the surface anchoring of C18 chains. This can be accomplished utilizing a dilute mixture of 1mM octadecyltrichlorosilane (OTS) in such liquid media as chloroform, hexadecane, toluene, or dichloromethane.[112] Silicon wafer pieces were submerged into the solution for 12 hours to allow self-assembly of the C18 onto the surface. These wafers were then removed and rinsed off with chloroform, 2-propanol, and deionized water. As indicated in Figure 6-5, the wafers exhibited long-lasting hydrophobic surfaces similar to those reverse phase C18-modified silica. The interactions of a C18 silica colloid probe with the silicon wafers would allow for an analogue to hydrophobic silica particle interactions in various environments, and further extend the ability to tailor interactions using liquids. However, difficulties would be encountered on how to go about modeling the dielectric response behavior of the C18 surface since in such a system the C18 configuration might change depending on solvents used and result in particle/interaction size difference in one solvent versus another.

Finally, though porous silica spheres were used, the effect of porosity on the interaction remains unknown. The porous features didn't seem to affect the interactions between silica and stainless steel walls in pure solvents, however, there might be an effect of solvent trapping in the pores during studies using mixed solvents or during a solvent exchange process. Thus, further work could be done to compare the effects of porosity on colloid interactions using dense silica spheres manufactured through various acid-catalyzed sol gel processes which can facilitate the production of micron-sized dense silica particles.[113-115]

Overall, exciting opportunities exist to further understand and facilitate the development of polymer dispersant-free systems through the use of the colloid probe system with the AFM. With ceramics manufacturing occurring on a world-wide industrial scale, shifting to a solvents system for traditional ceramics would decrease the production of greenhouse gases during final burn off and sintering. Furthermore, the use of solvents with low vaporization temperatures can be easily evaporated and condensed leading to the ability to recover and reuse the solvent for an eventual cost savings.

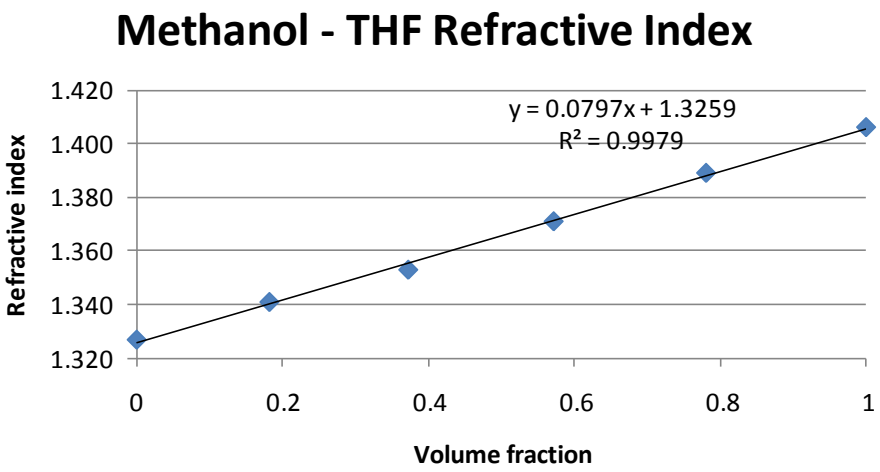

Figure 6-1. Refractive index measurement of THF in methanol.

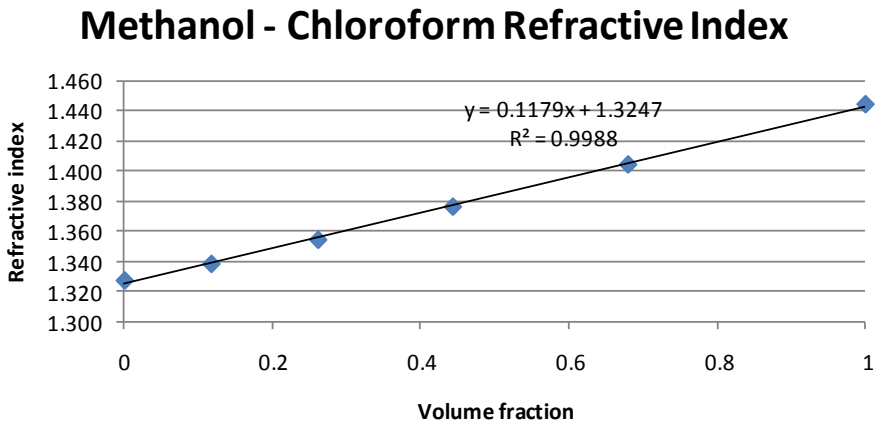

Figure 6-2. Refractive index measurement of chloroform in methanol.

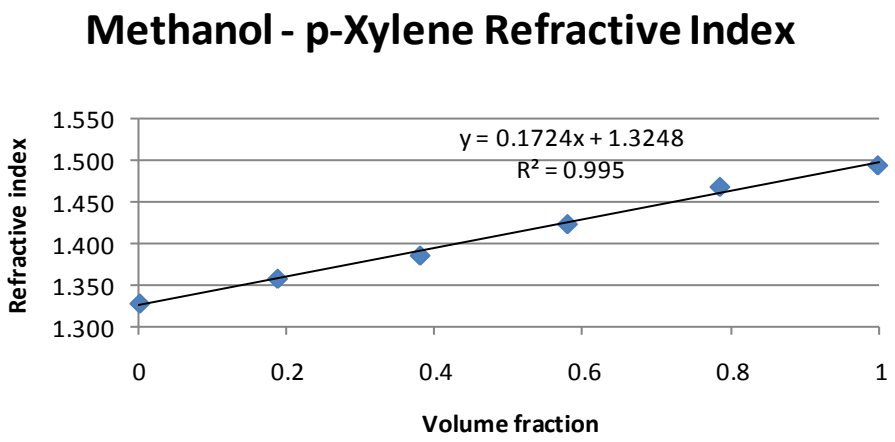

Figure 6-3. Refractive index measurement of p-xylene in methanol.

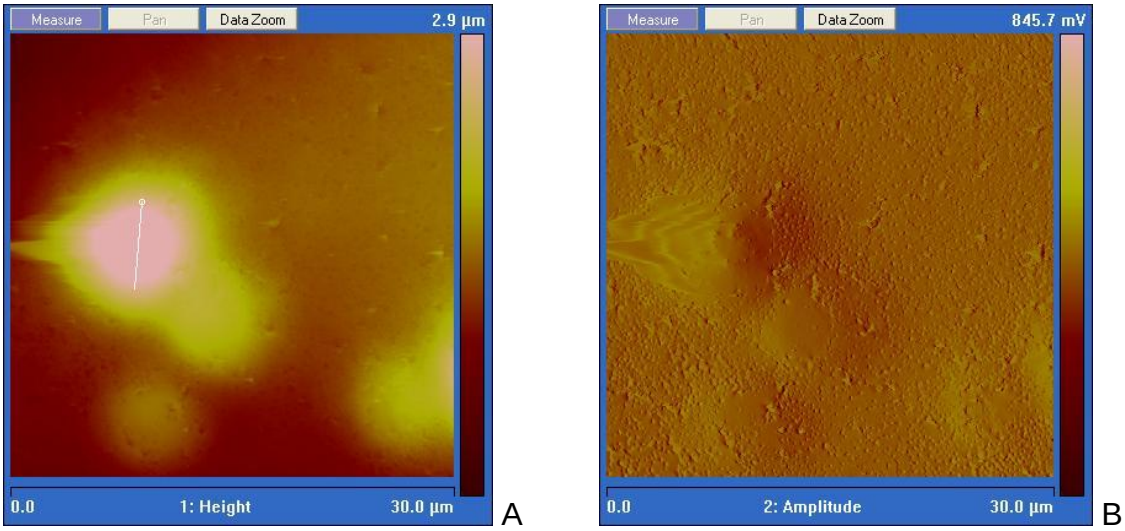

Figure 6-4. Tapping mode AFM of silica particles embedded into epoxy. A) Raw height information. B) Amplitude information to enhance contrast of topographic features.

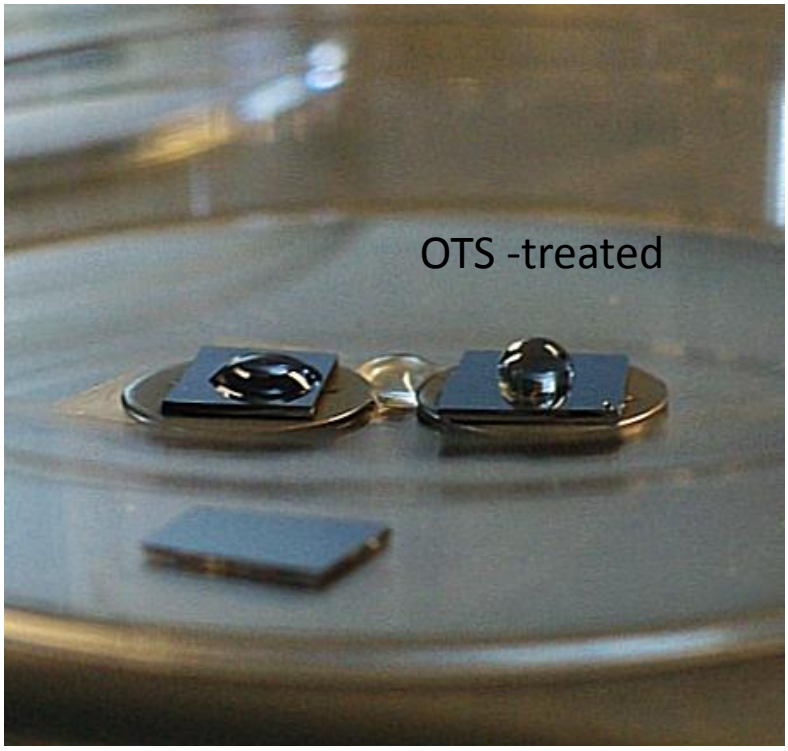

Figure 6-5. Comparison of water droplet on silicon wafer and wafer which has been treated with OTS.

LIST OF REFERENCES

(1) Rahaman, M. N. *Ceramic processing and sintering*; M. Dekker: New York, 1995.

(2) *2006-2007 China ceramic industry report*, Research In China, 2007.

(3) *National Strategies and China Ceramics Industry in the Future*, Casa, 2010.

(4) *Pearl River Delta Monitoring Results in 2007*, Hong Kong Regional Air Quality Monitoring Network, 2007.

(5) Israelachvili, J. N. *Intermolecular and surface forces*; 2nd ed.; Academic Press: Burlington, MA, 1991.

(6) Myers, D. *Surfaces, interfaces, and colloids : principles and applications*; 2nd ed.; Wiley-VCH: New York, 1999.

(7) Hamaker, H. C. *Physica* **1937**, *4*, 1058.

(8) Hamaker, H. C. *Recueil Des Travaux Chimiques Des Pays-Bas* **1937**, *56*, 727.

(9) Schroeder, P. R. *Chemical Clarification Methods for Confined Dredged Material Disposal*, US Army Engineer Waterways Experiment Station, 1983.

(10) Ninham, B. W. *Advances in Colloid and Interface Science* **1999**, *83*, 1.

(11) Adler, J. J.; Rabinovich, Y. I.; Moudgil, B. M. *J Colloid Interf Sci* **2001**, *237*, 249.

(12) Boinovich, L. *Curr Opin Colloid In* **2010**, *15*, 297.

(13) Grasso, D.; Subramaniam, K.; Butkus, M.; Strevett, K.; Bergendahl, J. *Reviews in Environmental Science and Biotechnology* **2002**, *1*, 17.

(14) Meyer, E. E.; Rosenberg, K. J.; Israelachvili, J. *Proceedings of the National Academy of Sciences of the United States of America* **2006**, *103*, 15739.

(15) Molina-Bolivar, J. A.; Galisteo-Gonzalez, F.; Hidalgo-Alvarez, R. *Colloid Surface B* **1999**, *14*, 3.

(16) Bhushan, B. *Handbook of micro/nanotribology*; 2nd ed.; CRC Press: Boca Raton, 1999.

(17) Colic, M.; Fisher, M. L.; Franks, G. V. *Langmuir* **1998**, *14*, 6107.

(18) Rabinovich, Y. I.; Derjaguin, B. V.; Churaev, N. V. *Advances in Colloid and Interface Science* **1982**, *16*, 63.

(19) Yotsumoto, H.; Yoon, R. H. *J Colloid Interf Sci* **1993**, *157*, 434.

(20) Tadros, T. F.; Lyklema, J. *J Electroanal Chem* **1969**, *22*, 1.

(21) Russel, W. B.; Saville, D. A.; Schowalter, W. R. *Colloidal dispersions*; Cambridge University Press: Cambridge ; New York, 1989.

(22) White, L. R. *J Colloid Interf Sci* **1983**, *95*, 286.

(23) Bhattacharjee, S.; Elimelech, M. *J Colloid Interf Sci* **1997**, *193*, 273.

(24) Huang, X. F.; Bhattacharjee, S.; Hoek, E. M. V. *Langmuir* **2010**, *26*, 2528.

(25) Martines, E.; Csaderova, L.; Morgan, H.; Curtis, A. S. G.; Riehle, M. O. *Colloid Surface A* **2008**, *318*, 45.

(26) Toikka, G.; Hayes, R. A.; Ralston, J. *Langmuir* **1996**, *12*, 3783.

(27) Hoek, E. M. V.; Agarwal, G. K. *J Colloid Interf Sci* **2006**, *298*, 50.

(28) Bergenholtz, J. *Curr Opin Colloid In* **2001**, *6*, 484.

(29) Vissers, J. P. C.; Laven, J.; Claessens, H. A.; Cramers, C. A.; Agterof, W. G. M. *Colloid Surface A* **1997**, *126*, 33.

(30) Greenwood, R. *Advances in Colloid and Interface Science* **2003**, *106*, 55.

(31) Hartley, P. G.; Larson, I.; Scales, P. J. *Langmuir* **1997**, *13*, 2207.

(32) Kosmulski, M.; Eriksson, P.; Brancewicz, C.; Rosenholm, J. B. *Colloids and Surfaces A: Physicochemical and Engineering Aspects* **2000**, *162*, 37.

(33) Vespalec, R.; Neca, J.; Simek, Z. *Colloids and Surfaces A: Physicochemical and Engineering Aspects* **1994**, *92*, 147.

(34) Xu, R. *Particle characterization : light scattering methods*; Kluwer Academic: New York, 2002.

(35) Krupp, H. *Advances in Colloid and Interface Science* **1967**, *1*, 111.

(36) Jiang, Y. B.; Matsusaka, S.; Masuda, H.; Qian, Y. *Powder Technology* **2008**, *186*, 199.

(37) Jiang, Y. B.; Matsusaka, S.; Masuda, H.; Yokoyama, T. *Advanced Powder Technology* **2006**, *17*, 413.

(38) Hein, K.; Hucke, T.; Stintz, M.; Ripperger, S. *Particle & Particle Systems Characterization* **2002**, *19*, 269.

(39) Craig, V. S. J. *Colloid Surface A* **1997**, *130*, 75.

(40) Tomlinson, G. A. *Philosophical Magazine* **1928**, *6*, 695.

(41) Rayleigh *Proceedings of the Royal Society of London Series a-Mathematical and Physical Sciences* **1937**, *160*, 0507.

(42) Derjaguin, B. V.; Titijevskaia, A. S.; Abricossova, I. I.; Malkina, A. D. *Discussions of the Faraday Society* **1954**, 24.

(43) Tabor, D.; Winterton, R. H. *Proceedings of the Royal Society of London Series a-Mathematical and Physical Sciences* **1969**, *312*, 435.

(44) Tabor, D.; Winterton, R. H. *Nature* **1968**, *219*, 1120.

(45) Israelachvili, J. N.; Tabor, D. *Proceedings of the Royal Society of London Series A-Mathematical and Physical Sciences* **1972**, *331*, 19.

(46) Israelachvili, J. N.; Tabor, D. *Nature-Physical Science* **1972**, *236*, 106.

(47) Hunkling.S; Arnold, W.; Geisselm.H *Review of Scientific Instruments* **1972**, *43*, 584.

(48) Derjaguin, B. V.; Kabanov, B. N.; Voropaye.Tn; Titiyevs.As *Journal of Colloid Science* **1964**, *19*, 113.

(49) Binnig, G.; Gerber, C.; Stoll, E.; Albrecht, T. R.; Quate, C. F. *Surface Science* **1987**, *189*, 1.

(50) Binnig, G.; Quate, C. F.; Gerber, C. *Physical Review Letters* **1986**, *56*, 930.

(51) Ducker, W. A.; Senden, T. J.; Pashley, R. M. *Nature* **1991**, *353*, 239.

(52) Ducker, W. A.; Senden, T. J.; Pashley, R. M. *Langmuir* **1992**, *8*, 1831.

(53) Lifshitz, E. M. *Soviet Physics* **1956**, *2*, 73.

(54) Parsegia.Va; Ninham, B. W. *Biophysical Journal* **1970**, *10*, 664.

(55) Parsegian, V. A. *Van der Waals forces : A handbook for biologists, chemists, engineers, and physicists*; Cambridge University Press: New York, 2006.

(56) Hough, D. B.; White, L. R. *Advances in Colloid and Interface Science* **1980**, *14*, 3.

(57) Bergstrom, L. *Advances in Colloid and Interface Science* **1997**, *70*, 125.

(58) Dzyaloshinskii, I. E.; Lifshitz, E. M.; Pitaevskii, L. P. *Advances in Physics* **1961**, *10*, 165.

(59) Blake, T. D. *Journal of the Chemical Society-Faraday Transactions I* **1975**, *71*, 192.

(60) Gee, M. L.; Healy, T. W.; White, L. R. *J Colloid Interf Sci* **1989**, *131*, 18.

(61) Van Oss, C. J.; Absolom, D. R.; Neumann, A. W. *Colloids and Surfaces* **1980**, *1*, 45.

(62) Milling, A.; Mulvaney, P.; Larson, I. *J Colloid Interf Sci* **1996**, *180*, 460.

(63) Meurk, A.; Luckham, P. F.; Bergstrom, L. *Langmuir* **1997**, *13*, 3896.

(64) Lee, S.; Sigmund, W. M. *J Colloid Interf Sci* **2001**, *243*, 365.

(65) Lee, S. W.; Sigmund, W. M. *Colloid Surface A* **2002**, *204*, 43.

(66) Cho, Y. K.; Wartena, R.; Tobias, S. M.; Chiang, Y. M. *Advanced Functional Materials* **2007**, *17*, 379.

(67) Feiler, A. A.; Bergstrom, L.; Rutland, M. W. *Langmuir* **2008**, *24*, 2274.

(68) Munday, J. N.; Capasso, F.; Parsegian, V. A. *Nature* **2009**, *457*, 170.

(69) Munday, J. N.; Capasso, F. *International Journal of Modern Physics A* **2010**, *25*, 2252.

(70) Houmard, M.; Berthome, G.; Boulange, L.; Joud, J. C. *Corrosion Science* **2007**, *49*, 2602.

(71) Kerber, S. J.; Tverberg, J. *Advanced Materials & Processes* **2000**, *158*, 33.

(72) Bertie, J. E.; Lan, Z. D. *Applied Spectroscopy* **1996**, *50*, 1047.

(73) Dagastine, R. R.; Prieve, D. C.; White, L. R. *J Colloid Interf Sci* **2000**, *231*, 351.

(74) Hale, G. M.; Querry, M. R. *Applied Optics* **1973**, *12*, 555.

(75) Hayashi, H.; Watanabe, N.; Udagawa, Y.; Kao, C. C. *Proceedings of the National Academy of Sciences of the United States of America* **2000**, *97*, 6264.

(76) Bell, N. S.; Dimos, D. B. In *Materials Research Society Spring 2000 Meeting* San Francisco, CA, 2000, p 6.

(77) Neto, C.; Craig, V. S. J. *Langmuir* **2001**, *17*, 2097.

(78) Hutter, J. L.; Bechhoefer, J. *Review of Scientific Instruments* **1993**, *64*, 1868.

(79) Ohler, B. *Review of Scientific Instruments* **2007**, *78*.

(80) Poggi, M. A.; McFarland, A. W.; Colton, J. S.; Bottomley, L. A. *Analytical Chemistry* **2005**, *77*, 1192.

(81) Chen, G. Y.; Warmack, R. J.; Huang, A.; Thundat, T. *Journal of Applied Physics* **1995**, *78*, 1465.

(82) Chen, G. Y.; Warmack, R. J.; Thundat, T.; Allison, D. P.; Huang, A. *Review of Scientific Instruments* **1994**, *65*, 2532.

(83) Sader, J. E. *Review of Scientific Instruments* **1995**, *66*, 4583.

(84) Sader, J. E.; White, L. *Journal of Applied Physics* **1993**, *74*, 1.

(85) Gibson, C. T.; Watson, G. S.; Myhra, S. *Nanotechnology* **1996**, *7*, 259.

(86) Senden, T. J.; Ducker, W. A. *Langmuir* **1994**, *10*, 1003.

(87) Torii, A.; Sasaki, M.; Hane, K.; Okuma, S. *Measurement Science & Technology* **1996**, *7*, 179.

(88) Cleveland, J. P.; Manne, S.; Bocek, D.; Hansma, P. K. *Review of Scientific Instruments* **1993**, *64*, 403.

(89) Sader, J. E.; Larson, I.; Mulvaney, P.; White, L. R. *Review of Scientific Instruments* **1995**, *66*, 3789.

(90) Eaton, P. J.; West, P. *Atomic force microscopy*; Oxford University Press: Oxford ; New York, 2010.

(91) Jaschke, M.; Butt, H. J. *Review of Scientific Instruments* **1995**, *66*, 1258.

(92) Weisenhorn, A. L.; Maivald, P.; Butt, H. J.; Hansma, P. K. *Physical Review B* **1992**, *45*, 11226.

(93) Kobayashi, M.; Juillerat, F.; Galletto, P.; Bowen, P.; Borkovec, M. *Langmuir* **2005**, *21*, 5761.

(94) Hoh, J. H.; Engel, A. *Langmuir* **1993**, *9*, 3310.

(95) Cappella, B.; Dietler, G. *Surface Science Reports* **1999**, *34*, 1.

(96) Kirkland, J. J.; DeStefano, J. J. *Journal of Chromatography A* **2006**, *1126*, 50.

(97) Bhushan, B. *Springer handbook of nanotechnology*; 2nd rev. & extended ed.; Springer: Berlin ; New York, 2007.

(98) Johnson, K. L.; Kendall, K.; Roberts, A. D. *Proceedings of the Royal Society of London Series a-Mathematical and Physical Sciences* **1971**, *324*, 301.

(99) Horn, R. G.; Smith, D. T.; Haller, W. *Chemical Physics Letters* **1989**, *162*, 404.

(100) Israelachvili, J.; Wennerstrom, H. *Nature* **1996**, *379*, 219.

(101) Rhodes, M. J. *Introduction to particle technology*; 2nd ed.; Wiley: Chichester, England ; Hoboken, NJ, 2008.

(102) Brinker, C. J.; Scherer, G. W. *Sol-gel science : the physics and chemistry of sol-gel processing*; Academic Press: Boston, 1990.

(103) Kittaka, S. *J Colloid Interf Sci* **1974**, *48*, 327.

(104) Parsegian, V. A.; Gingell, D. *Biophysical Journal* **1972**, *12*, 1192.

(105) Smallwood, I. M. *Handbook of Organic Solvent Properties*; Elsevier, 1996.

(106) Keir, R. I.; Suparno; Thomas, J. C. *Langmuir* **2002**, *18*, 1463.

(107) Vissers, J. P. C.; Claessens, H. A.; Laven, J.; Cramers, C. A. *Analytical Chemistry* **1995**, *67*, 2103.

(108) Unger, K. K. *Journal of Chromatography A* **2004**, *1060*, 1.

(109) *CRC handbook of chemistry and physics*; Chapman and Hall: Boca Raton, FL, 1999.

(110) Boyes, W. *Instrumentation reference book*; 3rd ed.; Butterworth-Heinemann: Boston, 2003.

(111) Deal, B. E.; Grove, A. S. *Journal of Applied Physics* **1965**, *36*, 3770.

(112) Cheng, Y. A.; Zheng, B.; Chuang, P. H.; Hsieh, S. C. *Langmuir* **2010**, *26*, 8256.

(113) Karmakar, B.; De, G.; Ganguli, D. *Journal of Non-Crystalline Solids* **2000**, *272*, 119.

(114) Karmakar, B.; De, G.; Kundu, D.; Ganguli, D. *Journal of Non-Crystalline Solids* **1991**, *135*, 29.

(115) Kawaguchi, T.; Ono, K. *Journal of Non-Crystalline Solids* **1990**, *121*, 383.

BIOGRAPHICAL SKETCH

Karran Woan has spent most of his educational career in the state of Florida. After graduating from Suncoast High School through the dual International Baccalaureate and Math, Science, and Engineering programs in 2001, he made his way to the University of Florida and enrolled in the Department of Materials Science and Engineering where he developed a fondness of materials characterization techniques. Nearing his last semester of undergraduate, he had the opportunity work with a materials research group at the Los Alamos National Laboratory. This experience cemented his desire to further pursue graduate research, which he continued at the University of Florida under Dr. Wolfgang Sigmund to research novel synthesis and characterization techniques. During his time in graduate school, Karran Woan applied for and was accepted to a 2-year NSF GK-12 program to enhance his communication skills of scientific concepts through a co-teaching position in a middle school science classroom. Karran Woan hopes to continue his career in fostering research and development of new technologies which will facilitate the improvement in the quality of life in the communities and world around him.